Brain Structure and Function (2020) 225:203–226
https://doi.org/10.1007/s00429-019-01997-4

ORIGINAL ARTICLE

Structural, morphometric and immunohistochemical study of the rabbit accessory olfactory bulb

Paula R. Villamayor[1] · Jose Manuel Cifuentes[1] · Luis Quintela[2] · Ramiro Barcia[3] · Pablo Sanchez-Quinteiro[1]

Received: 8 May 2019 / Accepted: 23 November 2019 / Published online: 4 December 2019

Abstract

The accessory olfactory bulb (AOB) is the first neural integrative centre of the vomeronasal system (VNS), which is associated primarily with the detection of semiochemicals. Although the rabbit is used as a model for the study of chemocommunication, these studies are hampered by the lack of knowledge regarding the topography, lamination, and neurochemical properties of the rabbit AOB. To fill this gap, we have employed histological stainings: lectin labelling with *Ulex europaeus* (UEA-I), *Bandeiraea simplicifolia* (BSI-B4), and *Lycopersicon esculentum* (LEA) agglutinins, and a range of immunohistochemical markers. Anti-G proteins Gαi2/Gαo, not previously studied in the rabbit AOB, are expressed following an antero-posterior zonal pattern. This places Lagomorpha among the small groups of mammals that conserve a double-path vomeronasal reception. Antibodies against olfactory marker protein (OMP), growth-associated protein-43 (GAP-43), glutaminase (GLS), microtubule-associated protein-2 (MAP-2), glial fibrillary-acidic protein (GFAP), calbindin (CB), and calretinin (CR) characterise the strata and the principal components of the BOA, demonstrating several singular features of the rabbit AOB. This diversity is accentuated by the presence of a unique organisation: four neuronal clusters in the accessory bulbar white matter, two of them not previously characterised in any species (the γ and δ groups). Our morphometric study of the AOB has found significant differences between sexes in the numerical density of principal cells, with larger values in females, a pattern completely opposite to that found in rats. In summary, the rabbit possesses a highly developed AOB, with many specific features that highlight the significant role played by chemocommunication among this species.

Keywords Accessory olfactory bulb · Vomeronasal system · Immunohistochemistry · Rabbits · Morphometry · Sexual dimorphism

Introduction

Chemical communication is one of the primary forms of communication that living beings use among themselves and with the environment (Wyatt 2003). The primary systems responsible for the detection of chemical molecules are the main olfactory system (MOS) and the accessory olfactory system (AOS) (Brennan & Zufall 2006; Swaney & Keverne 2009; Pardo-Bellver et al. 2017). Olfaction represents the most primitive sense in the majority of mammalian species and plays a crucial role during sexual and social behaviours, as well as spatial orientation (Brown 1985; Slotnick 2001; Ihara et al. 2013). The main olfactory epithelium (MOE) receptors have evolved to detect a broad range of odorants, while vomeronasal organ (VNO) receptors have evolved to detect limited groups of ligands, primarily intraspecific pheromonal cues but also a variety of heterospecific cues from sympatric competitors

Electronic supplementary material The online version of this article (https://doi.org/10.1007/s00429-019-01997-4) contains supplementary material, which is available to authorized users.

✉ Pablo Sanchez-Quinteiro
pablo.sanchez@usc.es

[1] Department of Anatomy, Animal Production and Clinical Veterinary Sciences, Faculty of Veterinary, University of Santiago de Compostela, Av Carballo Calero s/n, 27002 Lugo, Spain

[2] Department of Animal Pathology, Faculty of Veterinary, University of Santiago de Compostela, Lugo, Spain

[3] Department of Biochemistry and Molecular Biology, Faculty of Veterinary, University of Santiago de Compostela, Lugo, Spain

and predators (Grus et al. 2005; Ben-Shaul et al. 2010; Isogai et al. 2011). However, the AOS is well known to be capable of recognising other chemical signals, and the MOS is capable of detecting pheromones (Boehm 2006; Mandiyan et al. 2005; Yoon et al. 2005). This functional synergy between these two systems is likely associated with their structural similarities. Although the anatomical features between the two systems are well distinguished (Wysocki 1979; Halpern and Martínez-Marcos 2003), they are not completely morphologically independent, as demonstrated by not only the presence of vomeronasal receptors expressed in the olfactory mucosa and viceversa (Rodriguez et al. 2000, in humans; Sam et al. 2001 and Trinh & Storm 2003, both in mice), but also by their overlapping projections within the same subregions of the rat amygdala (Pro-Sistiaga et al. 2007).

In mammals, rabbits represent one of the best models for studying chemocommunication (González-Mariscal et al. 2016). Rabbits remain the only mammal species in which a mammary pheromone (MP; 2-methylbut-2-enal) has been fully characterised (Schaal et al. 2003). MP is released by lactating females to awaken rabbit neonates and initiate the nipple-sucking reflex. The fact that the receptors involved in the MP detection have still not been identified reflects the lack of knowledge on the anatomical and physiological basis of all the structures involved in rabbits chemocommunication. Although in 4-day-old rabbits, the detection of MP has been linked to the MOB by cFos studies (Charra et al. 2012), a similar approach at postnatal day 0 (Schneider et al. 2016) did not find activation in either the MOB or the AOB. These contradictory results remark the necessity of structural and morphofunctional studies of the chemosensory systems in rabbits, especially regarding the vomeronasal system, very crucial for reproduction and maternal behaviour in such closely related species as rodents (Keverne 2002). A necessary first step is to characterise the almost unexplored adult rabbit AOB.

Pheromones play a pivotal role in rabbits and can act as cues for submissive or dominant behaviours (Melo & González-Mariscal 2010). Because rabbits are often prey animals, olfaction is an essential sense for the detection of danger, predators, and potential mates (Apfelbach et al. 2005; Ben-Shaul et al. 2010). Recently, rabbits have increasingly been introduced as domesticated forms of livestock and pets and, in many areas of the world, they are part of daily life, in the forms of food, clothing and pets. Although the behavioural cues and reproductive features of rabbits have been investigated for decades (Verga et al. 2007; Szendrő et al. 2012), the techniques employed in these studies were primarily environment enrichment (Szendrő et al. 2013) or the induction of hormonal changes to enhance reproduction (Vega et al. 2012). Instead, studying pheromones appears to be a suitable method for improving the welfare of rabbits, reducing their stress levels and increasing their reproductive efficiency (Bouvier & Jacquinet 2008).

In Rodentia, the vomeronasal system (VNS) and its association with pheromone detection have been studied extensively, using morphological (Halpern 1987; Meisami & Bhatnagar 1998; Holy 2018), molecular (Mombaerts 2004; Zufall & Leinders-Zufall 2007; Isogai et al. 2011; Trouillet et al. 2019), and electrophysiological techniques (Mohrhardt et al. 2018), and these studies have demonstrated that the VNS play a pivotal role in species survival. Given the phylogenetic proximity between Lagomorpha (consisting of two families: Leporidae and Ochotonidae) and Rodentia, a greater knowledge of the VNS may demonstrate the importance of chemocommunication in rabbits and establish how both systems, MOB and AOB, can work together during communication between individuals of the same species.

Unfortunately, rabbit physiological and behavioural information has not been examined in concert with an exhaustive structural study of the VNS. The vomeronasal system is composed of the VNO, the AOB and the vomeronasal amygdala, and all of these are linked to each other through the vomeronasal nerves and tracts.

The primary structural features of the rabbit VNO have recently been studied in depth, showing a highly developed organ, with many specific morphological features and considerable immunohistochemical reactivity, suggesting that the organ is highly functional (Villamayor et al. 2018). However, there remains a lack of information regarding the structural and immunohistochemical properties of the AOB. Only a few studies are available, showing low-power histological images that appear to show a laminar structure (Segovia et al. 2006; Meisami & Bhatnagar 1998; Schneider et al. 2018), in addition to a few studies that have employed monoclonal antibodies against glycoconjugates (Mori 1987; Mori et al. 1987).

Although the AOB generally presents a laminar structure located caudally to the MOB, the AOB can have significant structural, phylogenetic, and species-specific variations among mammals (Meisami & Bhatnagar 1998). The AOB is completely developed in some species, such as rodents (Rodriguez et al. 1999), marsupials (Jia & Halpern 2004), and prosimians (Skeen & Hall 1977). In other species, such as the African elephant (Ngwenya et al. 2011), West Indian manatee (Mackay-Sim et al. 1985) and humans (Trotier et al. 2000), the AOB is absent or has not yet been identified, whereas in dogs (Salazar et al. 2013), mink (Salazar et al. 1998), and some bats (Frahm & Bhatnagar 1980), the AOB is present but appears to be poorly developed.

In the present work, a morphological and immunohistological analysis of the rabbit AOB was performed. We aimed to investigate the general features of the rabbit AOB at both the macroscopic and microscopic levels, to further our understanding of the anatomy of this component of the

VNS. Various tissue dissection and microdissection techniques were used, as well as general and specific histological stainings and lectin-histochemical labelling. We studied three lectins: *Ulex Europaeus* agglutinin (UEA), a specific marker for the vomeronasal pathway in several species (Salazar et al. 2013); *Bandeiraea simplicifolia* isolectin B4 (BSI-B4), a specific marker for the VNS in both rats (Salazar & Sanchez-Quinteiro 1998) and opossums (Shapiro et al. 1995); and *Lycopersicon esculentum* agglutinin (LEA), a specific marker for both olfactory systems.

In addition, an exhaustive immunohistochemical study was performed. We employed a wide variety of antibodies, for the first time, to examine the rabbit olfactory bulb. Among these antibodies, antibodies against G proteins are especially useful, as Gαi2 and Gαo subunit expression has been associated with the functional activity of the vomeronasal receptor families V1R and V2R, respectively (Shinohara et al. 1992; Jia & Halpern 1996). The primary neuronal elements of the bulb were characterised using microtubule-associated protein 2 (MAP-2) and α-glutaminase (GLS) antibodies. The neuronal growth and maturation were demonstrated by examining anti-growth-associated protein 43 (GAP-43), and anti-olfactory marker protein (OMP) staining, respectively. Antibodies against calbindin (CB) and calretinin (CR), which are both calcium-binding proteins, recognised proteins expressed in large quantities in both olfactory bulbs. Finally, an antibody against glial fibrillary acidic protein (GFAP) was employed as a marker of astrocytes and ensheathing cells.

The examination of the neuronal organisation of the rabbit AOB was completed with the microscopical study of the neuronal clusters encased within the accessory bulbar white matter, immediately beneath the AOB internal cellular layer (ICL). Following their first description by Ramón y Cajal (1904), these sub-bulbar structures have received very little attention. They only have been studied comprehensively in rats, mice, and guinea pigs by Larriva-Sahd (2012) who linked them with the transitional zone of the AOB. Our findings reveal that these sub-bulbar structures are more complexly organised in rabbits than has previously been described for other mammalian AOBs. With this study, we have addressed the existing knowledge gap regarding the structural and immunohistochemical characterisation of the first neural integrative centre of the VNS in rabbits.

Materials and methods

For the structural and immunohistochemical study, ten adult healthy rabbits of both sexes aged from at least 3.0 months to 1 year old. For the morphometric study, 12 adult healthy rabbits, 6 of each sex, aged 70 days old. All of them were provided by an abattoir and were commercial Hyplus hybrid (Grimaud Frères, France). The rabbits were humanely killed by electric shock under current legislation [Council Regulation (EC) 1099/2009], and the heads were separated from the carcasses in the slaughtering line. In addition, the intact heads from two adult BALB/c mice bred and euthanised for research in the Department of Pharmacy of the same faculty were kindly donated to the authors. They were used as a positive control in the immunohistochemical protocols. All procedures followed the guidelines for housing and handling provided by the Bioethical Committee of the University of Santiago de Compostela, and conformed to European legislation (EU directive 2010/63/EU) and Spanish legislation (RD 53/2013).

Two of the rabbit heads were dissected fresh for macroscopic studies of the anatomy of the vomeronasal system. The remaining heads were dissected only superficially and rapidly fixed by immersion in either 10% buffered formalin (Fr) or Bouin's fixative (Bn). In the latter case, after 24 h, the specimens were transferred to 70% ethanol. We performed all the experiments in both fixers and overall we found better results using Bn than Fr, apart from Tolivia and Bielschowsky stainings, which required Fr fixation.

After fixation, the olfactory bulbs (OBs) were completely dissected out for processing. Paraffin wax embedding was the most commonly performed type of inclusion. The OBs were cut into sagittal and transverse serial 5–8 µm sections for the examination of the AOB topography. The sections were stained with Nissl, Tolivia and Bielschowsky stainings. Immunohistochemical and lectin-histochemical stainings were performed in paraffin-embedded sections. Calcium-binding proteins' immunohistochemistry was additionally performed in free-floating sections. To perform the latter, after their fixation by immersion in either Fr or Bn, two unembedded bulbs were cryoprotected by immersion overnight at 4 °C in 30% sucrose in 0.1 M phosphate buffer (PB) and cut into 40-µm sagittal sections using a freezing microtome.

Tolivia protocol

The sections were mordanted for 1 h in 2.5% $(SO_4)_2FeNH_4$. The myelin staining solution was freshly prepared as follows: 5 ml of 20% hematoxylin plus 10 ml of 1% Li_2CO_3 in 50 ml of 50% ethanol. The slides were placed in the solution for 2.5 h. After 3 × 5 min washes, the samples were stained for 5 min in the following solution: 0.2% pyronine in 20% formaldehyde. Finally, the samples were dehydrated, cleared and mounted (Tolivia et al. 1998).

Bielschowsky's silver stain protocol

Dewaxed and hydrated slides were stained in 20% silver nitrate in dark at 37 °C for 30 min. After 2 × 5 min washes

in distilled water, concentrated ammonia was added to the silver solution drop by drop until the precipitate formed was completely dissolved. Samples were then incubated in this solution for 15 min at 37 °C in dark followed by 2 × 10 min 0.1% ammonia washes. The developer solution is made up of 20 ml formaldehyde 10%, 100 ml distilled water, 0.5 g citric acid, and 2 drops of nitric acid. Such solution was added to the initial silver solution and then the samples were rinsed in it for 10 min. The samples were washed again with ammonia and placed for 1 min in 5% sodium thiosulfate ($Na_2S_2O_3$). In some cases, the sections were counterstained with pyronin. Finally, the slides were washed in distilled water, dehydrated, cleared and mounted.

Lectin histochemistry protocol

The lectins LEA and BSI-B_4 were obtained as biotin conjugates from Vector (Vector Laboratories, Burlingame, CA, USA) and used as follows. (i) First, the sections were treated with 3% hydrogen peroxide in distilled water to quench endogenous peroxidase activity. (ii) Incubation for 30 min at room temperature with 2% bovine serum albumin (BSA) in 0.1 M Tris buffer (pH 7.2). (iii) The sections were incubated overnight at room temperature in the biotinylated lectins diluted in 0.5% BSA. (iv) The next day, the slides were incubated for 1.5 h at room temperature in Vectastain ABC reagent (Vector Laboratories, Burlingame, CA, USA). (v) Peroxidase activity was visualised by incubation in a solution containing 0.05% 3,3-diaminobenzidine (DAB) and 0.003% H_2O_2 in 0.2 M Tris–HCl buffer (pH 7.6) for 5 min. DAB was the chromogen and developed into a brown precipitate. Controls were run without lectin and with preabsorption of lectin by an excess amount of the corresponding sugar. Finally, the slides were dehydrated with alcohols, cleared in xylene and coverslipped.

Additionally, we used unconjugated UEA-I from Vector (Vector Laboratories, Burlingame, CA, USA). The steps (i) and (ii) were the same as above. (iii) The samples were incubated for 1 h at room temperature with the lectin UEA-I diluted in 0.5% BSA. (iv) Then, they were washed for 3 × 5 min in PB. (v) For 12 h, the samples were incubated with an immunoglobulin (Ig) against UEA conjugated to peroxidase (Dako, Denmark). (vi) The samples were washed in PB and (vii) they were finally incubated in DAB solution and dehydrated and mounted as above.

Controls were run both without lectin and with preabsorption of lectin by an excess amount of the corresponding sugar. None of these sections showed positive staining.

Immunohistochemical protocol for paraffin-embedded tissue

All primary antibody incubations were performed at 4 °C temperature while the secondary antibodies were incubated at room temperature. Both were kept in a humid chamber during the entire procedures. Unless otherwise stated, all washing steps consisted of three successive 5 min rinses in PB.

The sections were quenched in 3% H_2O_2 for 15 min. Next, non-specific binding was blocked for 30 min with either 2.5% horse normal serum of the ImmPRESS reagent kit Anti-mouse IgG/Anti-rabbit IgG (Vector Laboratories, Burlingame, CA, USA) or 2% BSA for 30 min (Table 1). ImmPRESS is a non-avidin–biotin polymer-based immunohistochemistry detection system which avoids the background staining due to endogenous biotin or avidin (Ramos-Vara &

Table 1 Antibodies and lectins used. Species of elaboration, dilutions, manufacturer, catalogue number

Ab/lectin*	1st Ab species/dilution	1st Ab catalogue number	2nd Ab species/dilution (catalogue number)
Anti-Gαo	Rabbit 1:100	MBL 551	ImmPRESS VR HRP Anti-rabbit IgG Reagent MP-6401-15
Anti-Gαi2	Rabbit 1:100	Sta Cruz biotechnology SC-7276	ImmPRESS VR HRP Anti-rabbit IgG Reagent MP-6401-15
Anti-OMP	Goat 1:400	Wako S44-10001	Horse 1:250 Vector BA-9500
Anti-MAP2	Mouse 1:200	Sigma M4403	ImmPRESS VR HRP Anti-mouse IgG Reagent MP-6402-15
Anti-GAP43	Mouse 1:800	Sigma G9264	ImmPRESS VR HRP Anti-mouse IgG Reagent MP-6402-15
Anti-GFAP	Rabbit 1:400	Dako Z0334	ImmPRESS VR HRP Anti-rabbit IgG Reagent MP-6401-15
Anti-GLUT	Rabbit 1:400	Abcam ab131554	ImmPRESS VR HRP Anti-rabbit IgG Reagent MP-6401-15
Anti-GABA	Rabbit 1:1000	ImmuSmol IS1006	ImmPRESS VR HRP Anti-rabbit IgG Reagent MP-6401-15
Anti-Calbindin	Rabbit 1:5000	Swant CB38	ImmPRESS VR HRP Anti-rabbit IgG Reagent MP-6401-15
Anti-Calretinin	Rabbit 1:5000	Swant 7697	ImmPRESS VR HRP Anti-rabbit IgG Reagent MP-6401-15
UEA-I*	1:10	Vector L-1060	Rabbit 1:50 DAKO P289
LEA*	20 µg/ml	Vector B-1175	Vectastain ABC reagent PK-4000
BSI-B_4*	100 µg/ml	Sigma L-2140	Vectastain ABC reagent PK-4000

For double immunostaining of both anti-Gαo (1:500) + anti-Gαi2 (1:200), and anti-MAP-2 (1:500) + anti-Gαi2 (1:200), the first and second antibodies were the same as those used for the single immunostaining

Miller 2006). The sections were then incubated overnight with the primary antibody. The next day, the samples previously blocked with the ImmPRESS kit were incubated for 20 min with either the corresponding ImmPRESS VR Polymer HRP Anti-Rabbit IgG Reagent or the Anti-Mouse IgG Reagent (Vector Laboratories). Those samples blocked in 2% BSA were instead washed and incubated in biotinylated secondary antibody raised against goat-IgG and after three washes they were incubated in Vectastain ABC reagent for 1.5 h. In all cases, after rinsing in 0.2 M Tris–HCl buffer (pH 7.6) for 10 min, the sections were finally developed using DAB as chromogen as we described for the lectin-histochemical labelling, and then dehydrated and mounted.

Double-immunohistochemical protocol for paraffin-embedded tissue

For double immnunostaining, a sequential twice-repeated enzyme-labeled method was employed (Hasui et al. 2003). Between both immunolabellings, the sections were subjected to treatment with 0.1 M glycine solution (pH 2.2) for 5 min. To select the most suitable dye to visualise the immunoreaction, both DAB and Vector VIP Peroxidase Substrate Kit (SK-4600, Vector Laboratories) were combined exchanging their order. Using first DAB and then VIP was the optimal combination for our immunostaining.

Immunohistochemical protocol for free-floating sections of unembedded tissue

Firstly, we performed an antigen retrieval step to expose the protein epitopes. The freezing microtome sections were placed at 80 °C for 30 min in 10 mM buffer, pH 6.0. From that point, the immunohistochemistry was similar to that followed in slide-mounted sections.

In all the immunohistochemical procedures, samples for which the primary antibody was omitted were used as negative controls, without obtaining labelling or unspecific background in any case. In addition, as positive controls, we replicated the immunohistochemical procedure with mouse tissues known to express the proteins of interest, obtaining the expected positive results.

Morphometric and stereological study

The OBs of the animals used in this part of the study, 12 rabbits, six from each sex, were immediately extracted and preserved in 10% formalin buffer. After paraffin embedding, the whole OBs were serial sectioned at 7 µm in the sagittal plane. The processing protocol was carefully standardised so that the samples treated followed an identical regime.

Morphometry

To estimate the volume of the AOB and MOB subdivisions, the Cavalieri principle was used. After serial sectioning of the whole OB, every 17th section for the AOB and every 40th for the MOB were selected for analysis. To ensure that the estimator is unbiased, the placement of the first section plane was chosen randomly. Ten to thirteen sections were sampled from each MOB, and ten to fourteen from each AOB following this systematic random manner. The sections were photomicrographed at low magnification (5× objective for AOB, and 1,20× for the MOB) and the boundaries and perimeters of each layer were manually outlined and digitised using a graphic pad (Intuos, Wacom) linked to a microcomputer.

After filling each layer with a pseudocolor (different grey levels for each layer), the total area of each region was determined using ImageJ software (ImageJ 1.52a, National Institutes of Health, USA). The total volume of each region was obtained by multiplying the sum of the areas of the individual profiles of each region by the number of sections measured and the distance between two sections. This distance was obtained from the product of the section thickness (7 µm) by the sampling interval.

A correction for tissue shrinkage during processing was applied (Mouton 2002). It required determining the change in area from the original unfixed state, to the sample on which the morphometry was performed. It corresponded to 1.8643.

Stereology

The number of cells for unit of volume was directly estimated by the physical dissector (Sterio 1984). After applying the dissectors over the photomicrographs of the 'reference sections', they were compared with their pairs ('look up' sections). To do this, 2 micrographs were made (20 × objective) of each paired section. According to the findings obtained from a pilot study, the first chosen section and its adjacent section were separated by a distance of 7 µm. The distance between the pair of sections must be about 30–40% of the average height of the object of interest.

Once the same histological area was located in both paired slices, the template with the dissectors (3–4 by section) was superposed on the reference image and the number of cells counted (Q-) of the reference image that fell within the counting frame without touching the forbidden lines (straight lines) and did not appear in the "look up" image. Finally, the number of dissectors (P) used was counted. The mean numerical density of cells was estimated using the following formula:

$$N_v = \frac{1}{\Delta x \cdot \Delta y \cdot h} \cdot \frac{\sum Q^-}{\sum P},$$

where $\Delta x \cdot \Delta y$ is the area of the dissector, h is the distance between paired sections of the dissector (in this case, 7 µm), ΣQ− is the sum of neurons counted according to the dissector, in every "volume section", and ΣP is the sum of dissectors used to measure the cells.

The number of sections studied varied from 10 to 13, depending on the bulb. In each section, 2–3 zones were studied and 2–4 dissectors were accounted for each.

Acquisition of images and digital processing

The digital images were captured with a Karl Zeiss Axiocam MRc5 digital camera paired to a Zeiss Axiophot microscope. Figures 1b–d, 3, 4, 5, 6, 7, 8, 9 and 11, 12, and 13 were then adjusted for fine-tune of the brightness and contrast and balance levels, applied to the whole image, using Adobe Photoshop CS4 (Adobe Systems, San Jose, CA, USA). In any case, no specific feature within an image was enhanced, moved or introduced. In addition, those figures which were made up of several photographs (Figs. 5a–b, 12a, 13a–d) were merged with an image-stitching software (PTGui Pro) and then cropped and resized using Photoshop. These mosaics are presented in supplementary material (Suppl. Figs. 7–8).

Results

Anatomical and histological study

The primary structures of the VNS are shown both macroscopically and microscopically in Fig. 1. The inner sensory neuroepithelium of the VNO is enclosed in a cartilaginous tubular structure located in the ventral part of the nasal septum (Fig. 1a, b). The nerve fibres of the vomeronasal nerves link the VNO to the brain (Fig. 1a, c). The AOB is the first relay station of the VNS. In rabbits, the AOB is located caudally and dorsally to the elongated main olfactory bulb (MOB) and ventrally to the frontal lobe (Fig. 1d). The thin amyelinic branches of the vomeronasal nerve are difficult to visualise macroscopically along their pathway through the submucosa of the nasal septum and intermingled with the olfactory nerves (Fig. 2a). After passing through the cribriform plate, the branches converge into a unique nerve that courses along the medial segment of the MOB (Fig. 2b), ending in a small elevation in the caudal-most part of the bulb, partially covered by the frontal lobe (Fig. 2c, d).

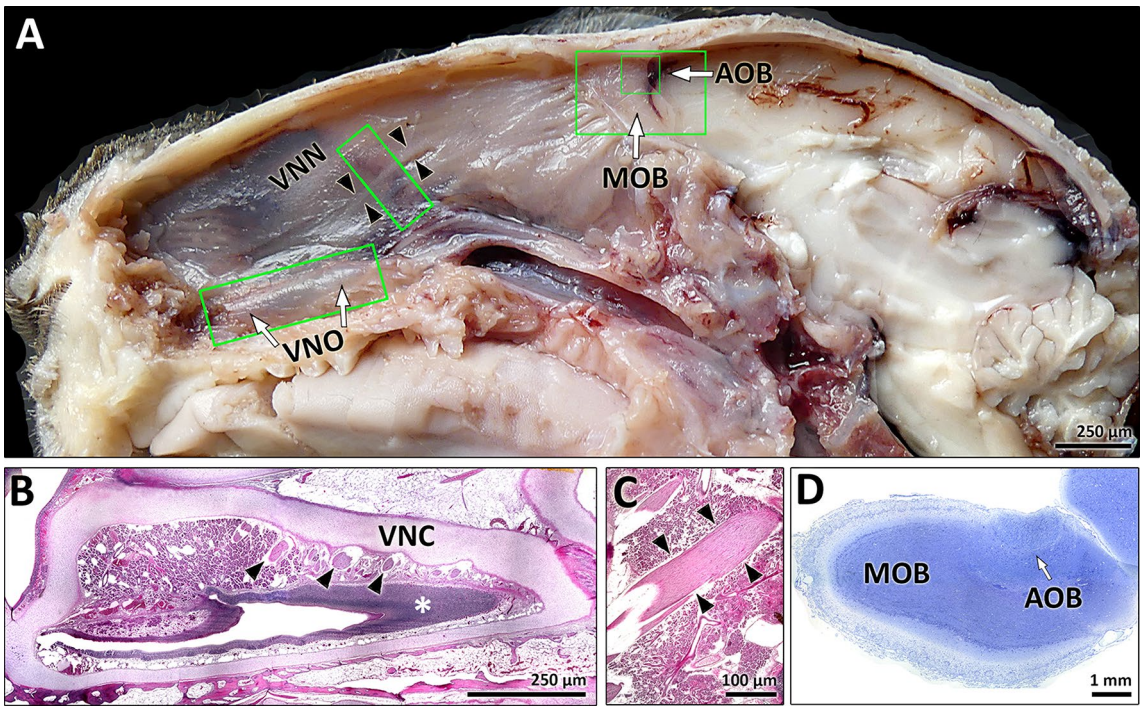

Fig. 1 VNS structures in the rabbit. **a** Mid-line sagittal section of the head of the rabbit showing the vomeronasal organ (VNO), the vomeronasal nerve (VNN) and the main olfactory bulb (MOB). **b** Sagittal histological section of the VNO, showing the vomeronasal neuroepithelium (asterisk), the cartilaginous capsule (VNC) and the branches of vomeronasal nerves leaving the organ dorsocaudally (arrowheads). **c** Amyelinic nerve branch of the VNN in the nasal septum (arrowheads). **d** Nissl-stained section of the olfactory bulb. *MOB* main olfactory bulb, *AOB* accessory olfactory bulb, *VNN* vomeronasal nerve, *VNC* vomeronasal cartilage, *VNO* vomeronasal organ

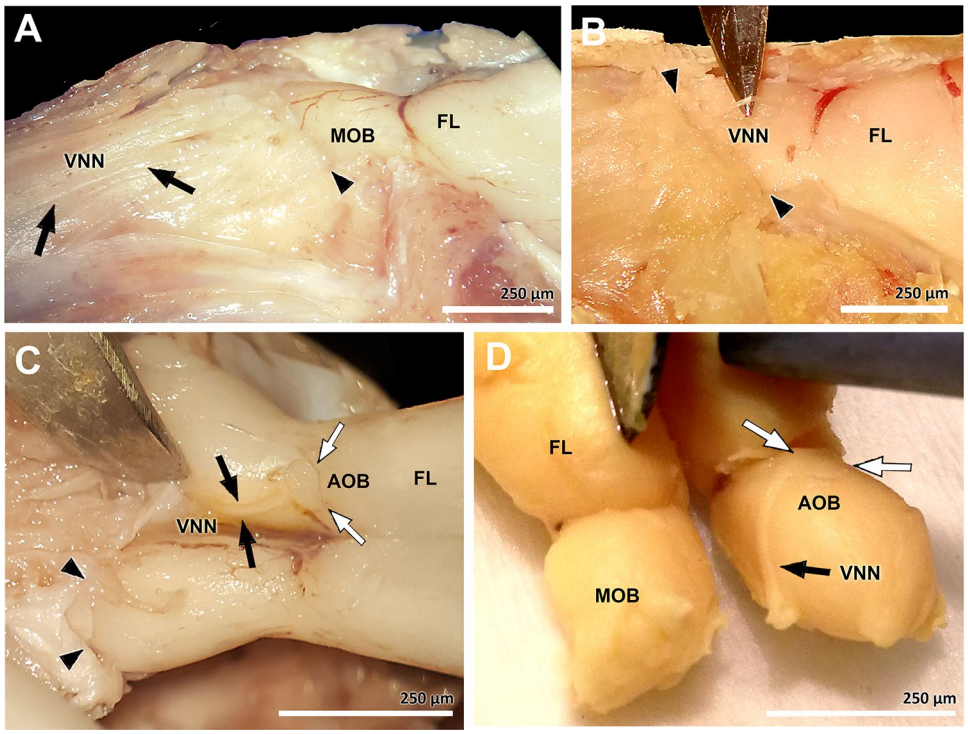

Fig. 2 Dissection of the vomeronasal nerve (VNN) and the accessory olfactory bulb (AOB). **a** Lateral view of the left nasal mucosa and anterior brain. The VNN is followed from its origin in the VNO, but it disappears when approaching the ethmoidal cribriform plate (arrowhead). **b** Medial view of the right olfactory bulb. The VNN is dissected out from the medial surface of the MOB. **c** Dorsal view of both olfactory bulbs, showing the arrival of the VNNs (black arrows) to the AOBs (white arrows). **d** Rostro-medial view of the left VNN and AOB. *FL* frontal lobe, *MOB* main olfactory bulb, *AOB* accessory olfactory bulb, *VNN* vomeronasal nerve

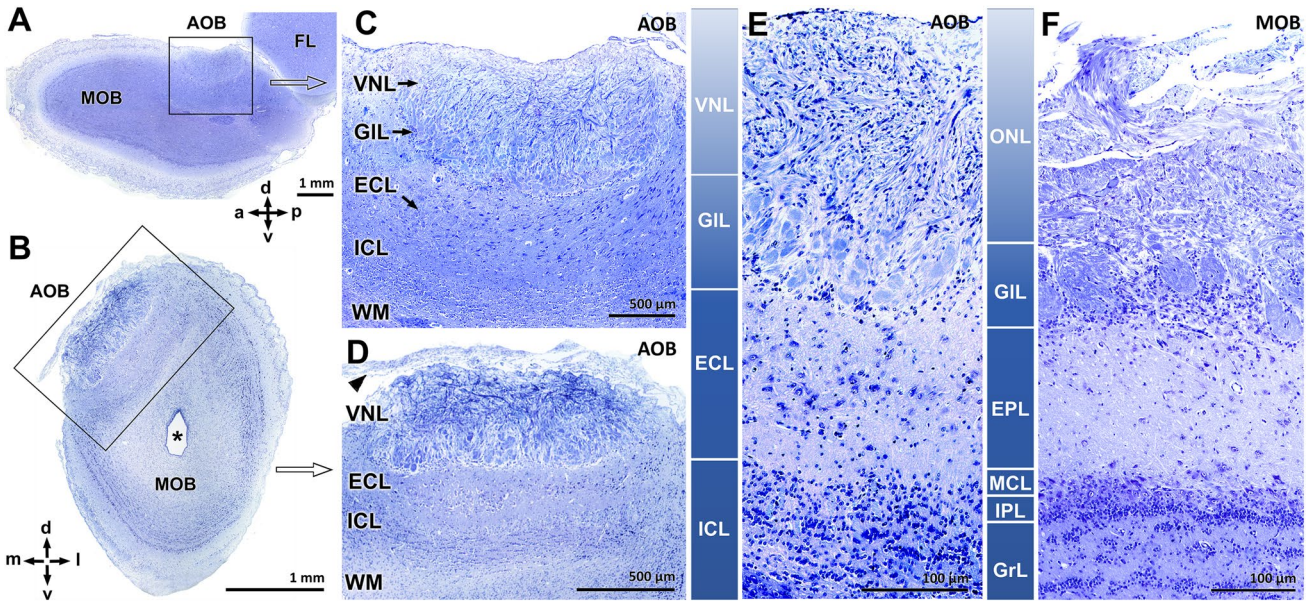

Fig. 3 Nissl-stained sections of the AOB. **a** Sagittal section of the olfactory bulb (OB) through the central axis of the AOB. **b** Transverse section of the OB through the central axis of the AOB showing the rostral horn of the lateral ventricle (*). **c** Higher magnification of the inset from (**a**). **d** Higher magnification of the inset from (**b**), showing the medial arrival of the VNNs to the AOBs (arrowheads). **e–f** Nissl-stained sections of the AOB (**e**) and MOB (**f**) showing the correspondence between their layers. *AOB* accessory olfactory bulb, *MOB* main olfactory bulb, *VNL* vomeronasal nerve layer, *ONL* olfactory nerve layer, *GlL* glomerular layer, *ECL* external cellular layer, *ICL* internal cellular layer, *EPL* external plexiform layer, *MCL* mitral cell layer, *IPL* internal plexiform layer, *GrL* granule cell layer, *FL* frontal lobe, *WM* white matter, *a* anterior, *p* posterior, *d* dorsal, *v* ventral, *m* medial, *l* lateral

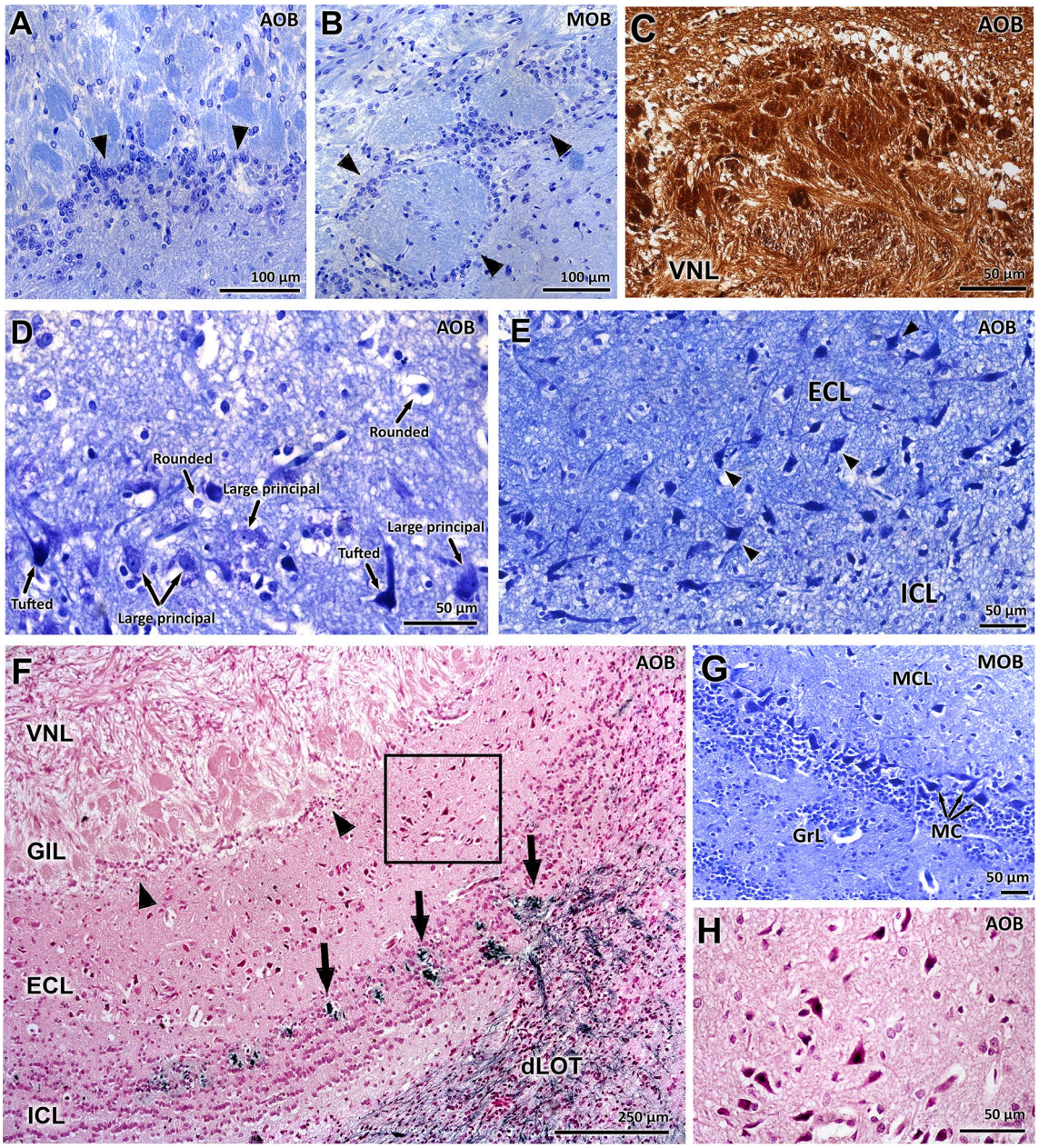

Fig. 4 Nissl (**a**, **b**, **d**, **e**, **g**), Bielschowsky (**c**), and Tolivia (**f**, **h**) stained sections of AOB layers. **a** Glomeruli of the AOB showing the periglomerular (PG) cells (arrowheads) concentrated along the deeper segment of the glomeruli. **b** Glomeruli of the MOB, well delineated around their perimeters by PG cells (arrowheads). **c** Bielschowsky staining shows how the fibres of the VNN embrace clusters of AOB glomeruli. **d** Main cellular types in the ECL: Large principal, rounded and tufted. In any case, they had mitral-like shape. **e** Tufted cells of the ECL frequently appeared concentrated. **f** External cellular layer (ECL) of the AOB, defined by the PG cells of the GlL (arrowheads) and the ICL. The arrows indicate the axonal fibres projecting from the ECL that overlay the ICL. These fibres constitute the contribution of the AOB to the dorsal peduncle of the lateral olfactory tract (dLOT). **g** Mitral cells of the MOB. **h** Higher magnification of the boxed area from D showing the principal cells of the ECL. *VNL* vomeronasal nerve layer, *GlL* glomerular layer, *ECL* external cellular layer, *ICL* internal cellular layer

The primary microscopical features of the AOB were studied using Nissl, Tolivia, and Bielschowsky staining techniques. Nissl staining showed a large, semi-oval, and well-laminated AOB, in both sagittal and transversal sections (Fig. 3a–d). The thickness and the sharpness of boundaries among the layers were neat. The outermost layer of the AOB is formed by the fibres of the vomeronasal nerves, which spread over the surface to form a definite fibre layer and then turn inward to shape the glomeruli. The glomeruli of the AOB are smaller than those of the MOB, and they are

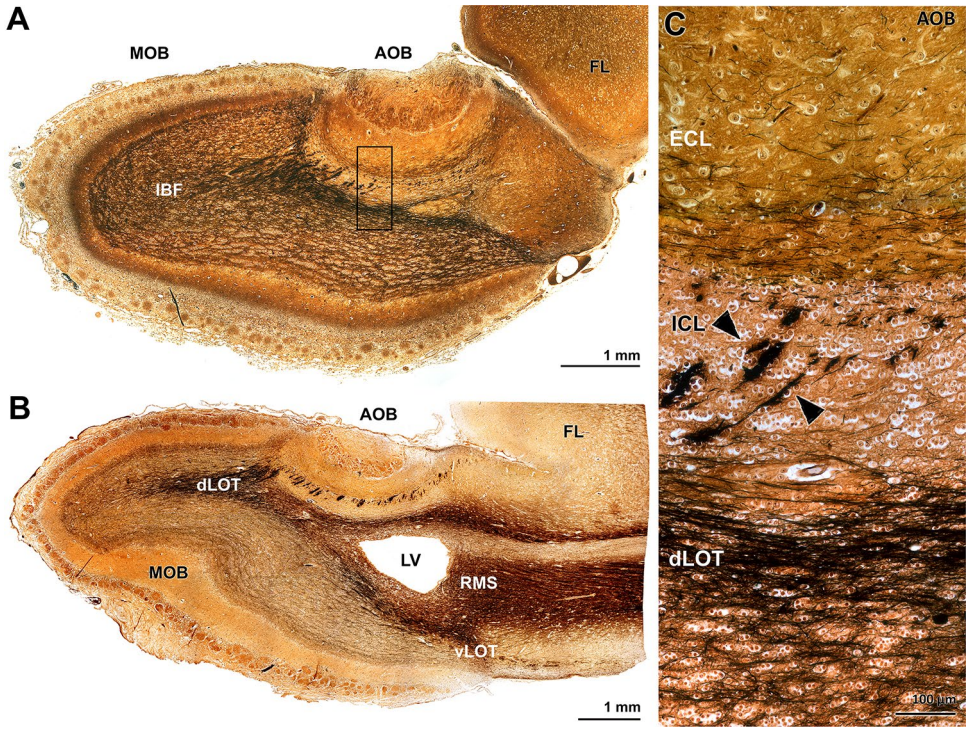

Fig. 5 Bielschowsky-stained sagittal sections of the AOB. **a** Sagittal section of the olfactory bulbs through the rostro-caudal axis of the AOB, showing its shape and layers, as well as the intrabulbar fibres (IBF) of the MOB. **b** Paramedian sagittal section of the OB, located laterally to the section displayed in (**a**), showing the main tracts of the bulb, the dorsal lateral olfactory tract (dLOT), ventral lateral olfactory tract (vLOT) and the rostral migratory stream (RMS). **c** Higher magnification of the inset from (**a**), showing the deeper layers of the AOB. The arrowheads show the myelinic fibres projecting from the external cellular layer (ECL), which constitute the contribution of the AOB to the dLOT. *FL* frontal lobe, *AOB* accessory olfactory bulb, *MOB* main olfactory bulb, *IBF* intrabulbar fibres, *dLOT* dorsal lateral olfactory tract, *RMS* rostral migratory stream, *vLOT* ventral lateral olfactory tract, *LV* rostral horn of the lateral ventricle, *ECL* external cellular layer, *ICL* internal cellular layer

densely packed. Although the organisation of the glomeruli in the AOB appears to be more diffuse than the organisation of the glomeruli in the MOB (Fig. 3e, f), Bielschowsky staining showed a supraglomerular organisation (Fig. 4c), which was not noticeable with Nissl staining. Whereas in the MOB the whole perimeter of the glomeruli is delimited by periglomerular cells (Fig. 4b), in the AOB, these cells are primarily concentrated along the border between the glomerular layer and ICL, forming a very narrow band (Fig. 4a).

To describe the deep layers of the AOB, we have adhered to the nomenclature proposed by Larriva-Sahd (2008) who avoids the customary use of terms taken from the description of the MOB. Neither the main cells of the AOB are mitral in shape nor is there an authentic plexiform layer. For that reason, we will use, following Larriva-Sahd, the term external cellular layer (ECL) for what has usually been called mitral-tufted layer, ICL for the granular layer, and principal cells instead of mitral cells.

Instead of a typical monolayer of mitral-like cells, the principal cells of the AOB are scattered along the broad ECL, which extends from the glomerular layer (GlL) to the internal cellular layer (ICL) (Figs. 3e, 4f). Both Nissl and Tolivia staining of the AOB principal cells (Fig. 4d, e, h) showed that they are not as characteristically mitral in shape as the mitral cells of the MOB (Fig. 4f). Instead, they show a variable morphology, with three main types: large principal cells, rounded cells, and tufted cells (Fig. 4d, e). Large principal cells have big ovoid nucleus with patent nucleolus and a large soma; rounded cells possess a smaller rounded nucleus, and tufted cells remember to the tufted cells of the MOB. The tufted cells are intensely stained by Nissl and Tolivia stainings (Fig. 4h), have a triangular shape and present a prominent primary dendrite. They are often concentrated in groups (Fig. 4e).

The ICL forms the deepest layer of the AOB. This layer contains medium-sized granule cells, grouped into islets, which are overlaid by the myelinic efferent fibres of the AOB, as demonstrated by both the Tolivia and Bielschowsky methods (Figs. 4f, 5a, b). These axonal fibres, which project from the ECL, constitute the contribution of the AOB to the dorsal peduncle of the lateral olfactory tract (LOT), which in rabbits passes under the ICL (Fig. 5c).

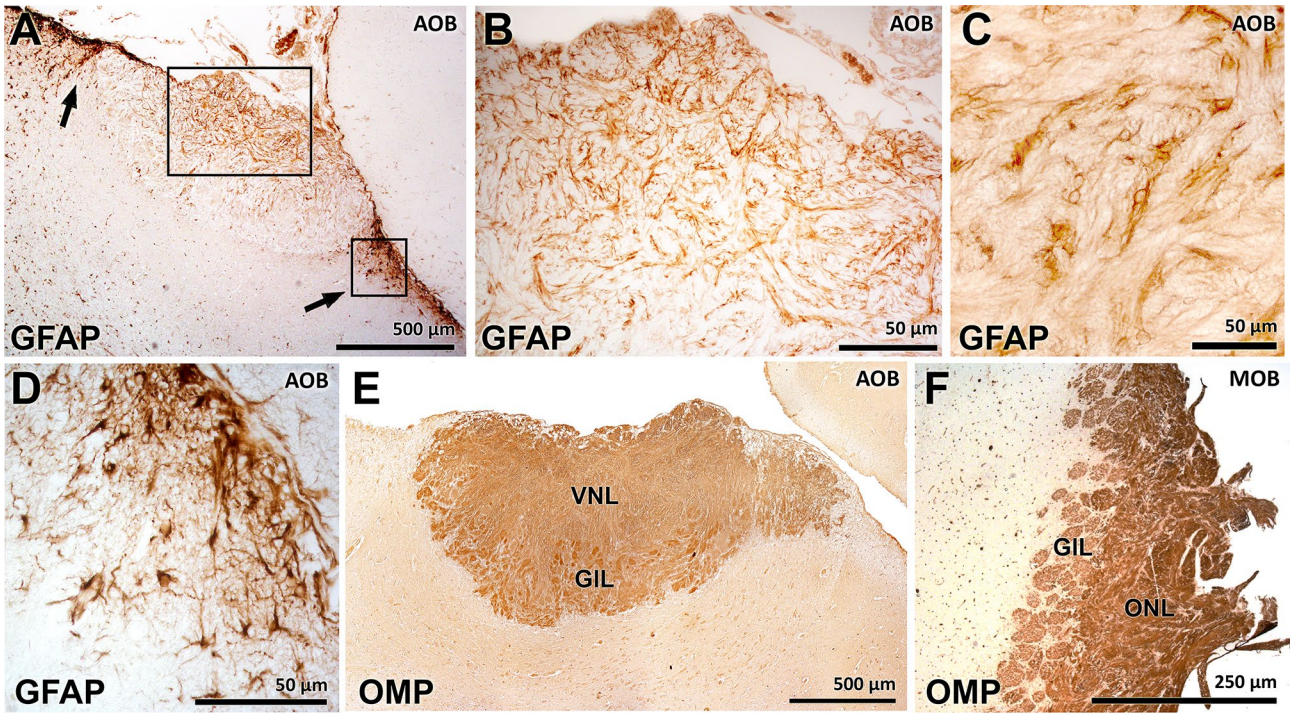

Fig. 6 Immunostaining for GFAP and OMP in the AOB. **a** Anti-GFAP staining was restricted to the VNL in the AOB. Additionally, there was a definite area of immunolabelling around the periphery of the AOB (arrows). **b** Higher magnification of the superior inset from (**a**) confirms the immunostaining of the processes of the vomeronasal ensheathing cells in the AOB neuropil. **c** Occasionally, the cell bodies of the ensheathing cells were discernible. **d** Higher magnification of the inferior inset from (**a**) shows a conspicuous presence of astrocytes external to the pial basement membrane that surrounds the AOB. **e** Anti-OMP uniformly stains both superficial layers of the AOB: the VNL and the GlL. **f** The anti-OMP immunolabelling also labels the corresponding layers of the MOB: the ONL and the GlL. *GFAP* glial fibrillary acidic protein, *OMP* olfactory marker protein, *VNL* vomeronasal nerve layer, *GlL* glomerular layer, *ONL* olfactory nerve layer

Immunohistochemical and lectin-histochemical study

Most of the immunohistochemical markers used in this study stained the superficial layers of the AOB, following different patterns. The immunostaining using the anti-GFAP antibody shows the glial components. The labelling was restricted to the vomeronasal nerve layer (VNL). Despite the lack of astrocytes, positive immunostaining of the processes from vomeronasal ensheathing cells was observed, surrounding and subdividing the neuropil (Fig. 6a–c). Moreover, in all the specimens studied, there was a noticeable concentration of astrocytes external to the pial basement membrane that surrounds the AOB (Fig. 6a, d).

The presence of olfactory marker protein (OMP), an olfactory neuron maturation marker, in both the AOB and the MOB was demonstrated by the binding of the anti-OMP antibody to the superficial layers of the whole bulb. The staining was constricted to the nerve and GlLs of both bulbs.

The expression of antibodies against G proteins, Gαi2 and Gαo subunits, has been associated with the functional activity of the main vomeronasal receptor families V1R and V2R, respectively. Double and single immunolabelling of the G protein subunits Gαi2 and Gαo showed that the expression patterns of both proteins in the superficial layers of the AOB follow a zonal segregation pattern (Fig. 7a–d). The antibody against Gαi2 stained only the anterior half of the VNL–GlL of the AOB, whereas the posterior half of both layers was not stained at all (Fig. 7a, c). The boundary between the stained anterior segment and the unstained posterior segment is sharp and clear. The antibody against Gαo stained the posterior half of the VNL–GlL. The anterior half of the nerve layers was not stained, although the glomeruli appeared to be partially stained (Fig. 7b, d). The staining of these latter glomeruli corresponds with the dendrites from neurons in the underlying layers of the AOB. The boundaries between the posterior and anterior segments of the VNL–GlL are also clear and sharp. Unlike the differential staining observed for the VNL–GlL of the AOB, the staining for Gαo is relatively uniform in other regions of the brain, including the ECL and ICL of the AOB and all layers in the MOB.

The anti-GAP-43 staining reflected a high level of axonal growth. The immunolabelling appears to be more intense in both the superficial and internal cellular layers of the AOB (Fig. 7f). In the superficial layers, GAP-43 staining revealed the zonal organisation of the AOB, with stronger

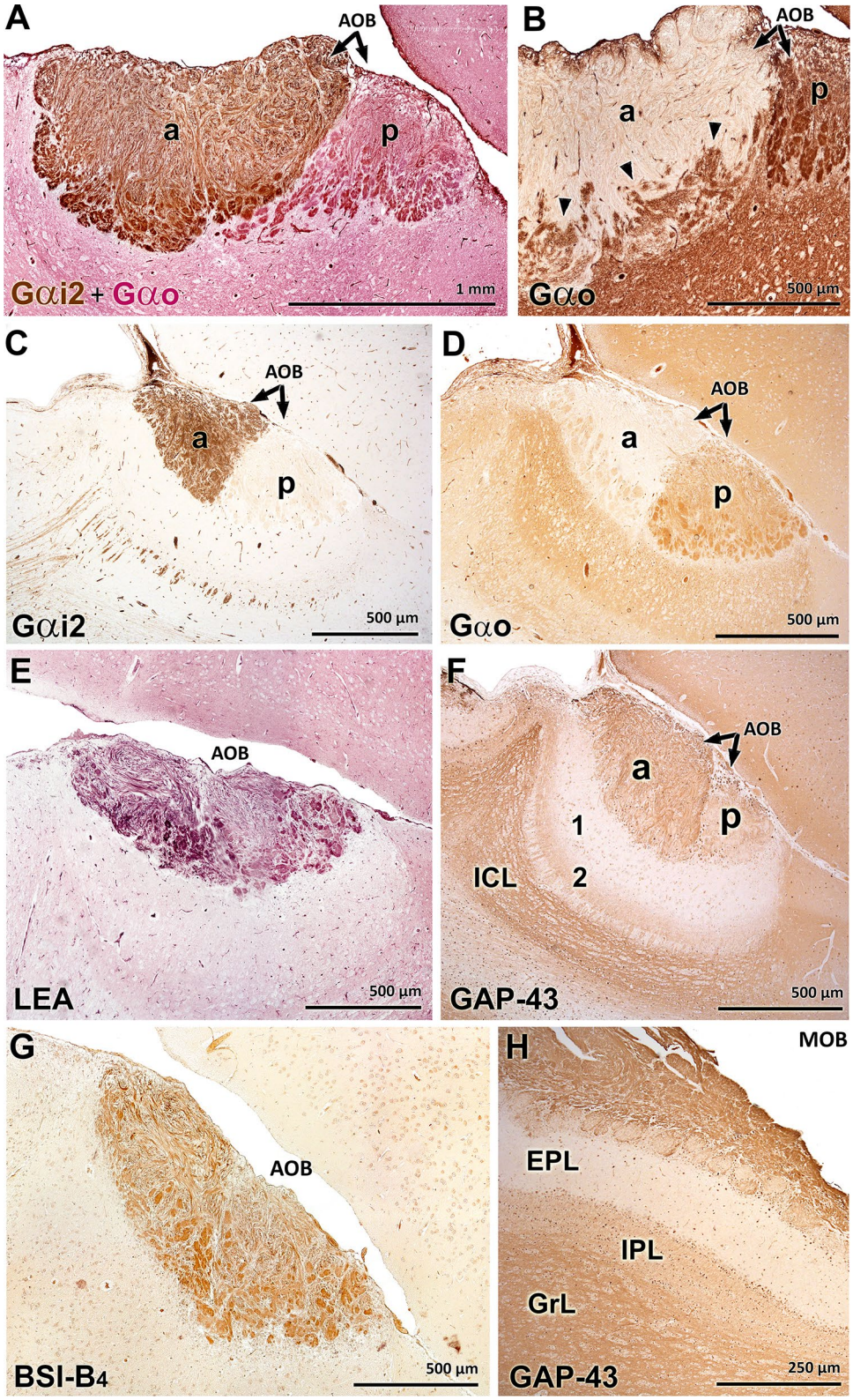

Fig. 7 Immunohistochemical labelling of the G proteins subunits and GAP-43 and the lectin-histochemical labelling of the OBs. **a** Double immunostaining for Gαi2 and Gαo in the AOB. Anti-Gαi2 (brown) stains the anterior half of the VNL and GlL of the AOB. Anti-Gαo (red) stains the posterior half of the VNL and GlL. **b** Single immunostaining with anti-Gαo showing glomeruli in the anterior half of the AOB that are partially stained. This labelling corresponds to the dendrites from neurons in the underlying layers of the AOB. **c** Simple immunolabelling with anti-Gαi2 stains the anterior VNL and GlL of the AOB. The posterior zone is devoid of labelling. **d** Simple immunolabelling with anti-Gαo stains the complementary posterior half of the VNL and GlL of the AOB. The anterior half of the VNL is not stained. As observed in (**b**), some glomeruli in the anterior half are stained. **e** LEA histochemical labelling of the AOB labels both vomeronasal axons and glomeruli in the whole AOB. **f** AOB immunostaining with anti-GAP-43 labels the superficial layer and the ICL. In the superficial layer anti-GAP43 labelling reveals an antero-posterior zonation. In the ECL, anti-GAP43 establishes a distinction between the presumptive EPL (1) and IPL (2). **g** BSI-B_4 histochemical labelling of the AOB produces a similar pattern as that observed with LEA labelling, staining the superficial layers of the whole AOB. **h** MOB immunostaining with anti-GAP-43 produces a pattern similar to that shown in (**f**) for the AOB, confirming the neat distinction between the EPL and the IPL. *a* anterior, *p* posterior, *ICL* internal cellular layer, *EPL* external plexiform layer, *IPL* internal plexiform layer, *VNL* vomeronasal nerve layer, *GlL* glomerular layer

labelling in the anterior zone than in the posterior zone, defining both areas very neatly. Moreover, in the MOB, anti-GAP-43 stained the internal plexiform layer (IPL) more strongly than the external plexiform layer (EPL) (Fig. 7h). This pattern was conserved in the AOB, establishing a distinction between the superficial and deep ECLs (Fig. 7f).

We used lectin-histochemical techniques to characterise the glycoconjugates expression in the superficial layers of

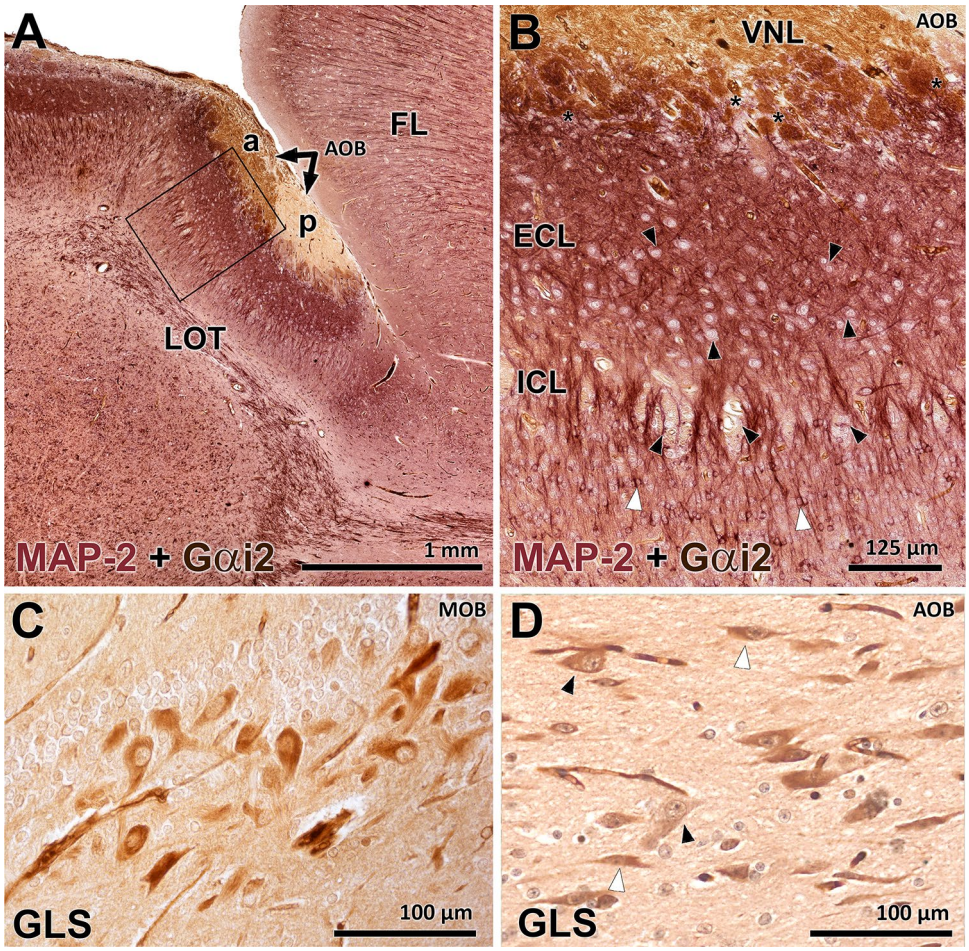

Fig. 8 Immunohistochemical labelling of MAP-2 and GLS in the OBs. **a** Double immunostaining with MAP-2 and Gαi2 antibodies in the AOB. Anti-MAP-2 (red) profusely stains the dendritic trees of principal/mitral cells of the AOB/MOB, respectively, and granular cells in both OBs, as well as the pyramidal cells in the frontal lobe (FL). **b** Higher magnification of the inset depicted in (**a**), showing the AOB layers. The contributions of both vomeronasal axons (brown) and principal cell dendritic trees to the glomeruli of the AOB (asterisks) are noticeable. The soma of the principal cells and the axons contributing to the dorsal peduncle of the lateral olfactory tract remain unlabelled (black arrowheads). The spherical cell bodies and processes of granule cells are immunolabelled (white arrowheads). **c** The mitral cells of the MCL of the MOB are immunopositive to anti-GLS. **d** Principal cells in the ECL of the AOB immunostained with anti-GLS. Both large principal (black arrowheads) and tufted cells (white arrowheads) are immunopositive. MAP-2, microtubule-associated protein 2; *GLS* glutaminase; *FL* frontal lobe, *LOT* lateral olfactory tract, *a* anterior, *p* posterior, *VNL* vomeronasal nerve layer, *ECL* external cellular layer, *ICL* internal cellular layer, *MCL*, mitral cellular layer

the rabbit AOB. The expression of such glycoconjugates varies among species allowing, in some cases, to characterise specifically both olfactory systems. Among the three lectins used, the N-acetylglucosamine-specific LEA (Fig. 7e), and the α-galactose-specific BSI-B_4 (Fig. 7g) stained the VNL and GlL of the AOB, without defining antero-posterior zonation. Both of these lectins also stained the corresponding layers of the MOB. The L-fucose-specific UEA did not stain any part of the olfactory bulb.

AOB principal cells were characterised not only with histological staining but also using antibodies against GLS and MAP-2. The former antibody labelled the somas of mitral cells in the MOB (Fig. 8c) and principal cells of the AOB, mostly those with elongated somas but also large principal cells (Fig. 8d). No type of AOB principal cells was immunolabelled with the antibody to GABA.

Anti-MAP-2 antibody is a useful marker for the dendritic trees of mitral/principal cells. The MAP-2 immunoreactivity infiltrated all the glomeruli in the AOB, but did not intermingle with the axons of the VNL, as shown by the double-immunohistochemical labelling with MAP-2 and Gαi2 antibodies (Fig. 8a, b). The immunolabelling was very dense in the ECL but did not affect the mitral cell somas. In the granule cells of the ICL, MAP-2 immunolabelled the spherical cell bodies and the processes that lead towards the superficial regions of the AOB.

The calcium-binding proteins CR and CB are valuable markers of neuronal subtypes. The antibodies against both

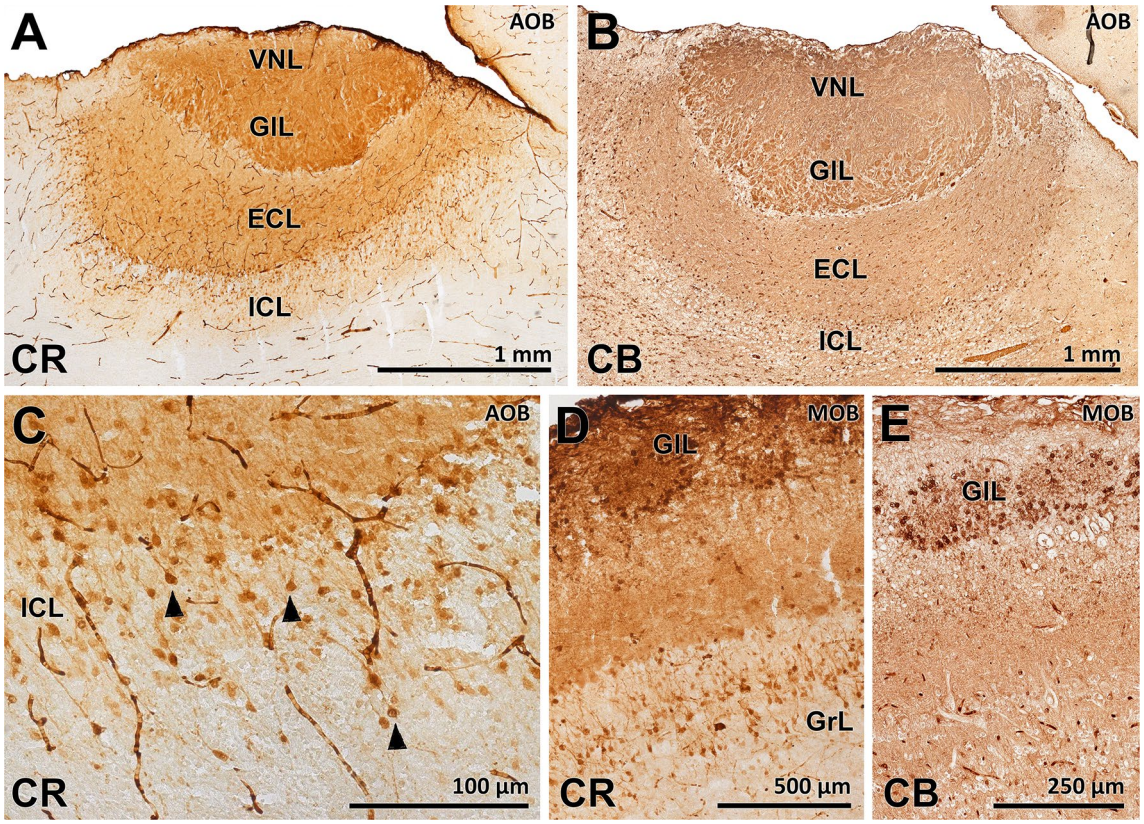

Fig. 9 Immunohistochemical labelling of calcium-binding proteins in the OBs. **a** Low-power sagittal section of the AOB immunostained with the antibody against CR. The superficial and middle layers show intense labelling of their neuropils. This staining appears to be stronger in the VNL and GlL. **b** AOB immunostained with anti-CB shows a pattern similar to that for anti-CR immunostaining. **c** The only cellular elements immunostained in the AOB are concentrated in the ICL, where the granule cells and their processes are stained by anti-CR. **d** In the MOB, anti-CR stains both the PG and granular cells, whereas CB immunostaining (**e**) labels only the PG cells. *VNL* vomeronasal nerve layer, *GlL* glomerular layer, *ECL* external cellular layer, *ICL* internal cellular layer, *CB* calbindin, *CR* calretinin

of them labelled the AOB. The staining was primarily concentrated in the neuropil of the superficial and middle layers (Fig. 9a, b). The periglomerular (PG) cells were not immunopositive, either in cryostat free-floating sections (Fig. 9a) or in paraffin-embedded sections (Fig. 9b). The absence of CB and CR PG cells in the AOB contrasts with their presence in the MOB, where the glomeruli are found to be neatly delineated by the immunopositive PG cells (Fig. 9d, e). Granule cells are labelled by both the antibodies against CR and anti-CB.

Neuronal clusters in the accessory bulbar core white matter

Nissl-stained serial sagittal sections of the bulb showed four distinct cellular clusters that contained pyramidal-like neurons parallel to the base of the AOB. These nuclei were encased in the accessory bulbar white matter of the LOT, immediately beneath the ICL. They follow an ordered topographical pattern that is demonstrated in Fig. 10. Two of these nuclei were located in the caudal half of the AOB, with one located medially and one located laterally. The other two nuclei were located at the level of the anterior third of the AOB, in a similar fashion, with one located medially and the other located laterally. The caudal nuclei correspond to what have been termed the α and β groups of the anterior olfactory nucleus (AON) (Valverde et al. 1989). The α group is situated in the medial aspect of the bulb, whereas the β cluster is located closer to the lateral surface. The two rostral nuclei are described here for the first time. One is located medially, while the other is located laterally. According to the criteria used to name the caudal nuclei, we have named these nuclei the γ and δ groups, respectively.

In all cases, the Nissl sagittal stainings (Figs. 11, 12a, b, 13) showed that the nuclei contain large, deeply stained, oval and polygonal cells. The presence of the four nuclei was also confirmed in our Nissl transverse serial sections (Fig. 13). Pyronin and Bielschowsky stains confirmed that the clusters are encapsulated by the thick fibres of the dorsal LOT (Fig. 12c, d). The immunohistochemical study showed that the nuclei are composed of GLS-immunoreactive cells (Fig. 12e).

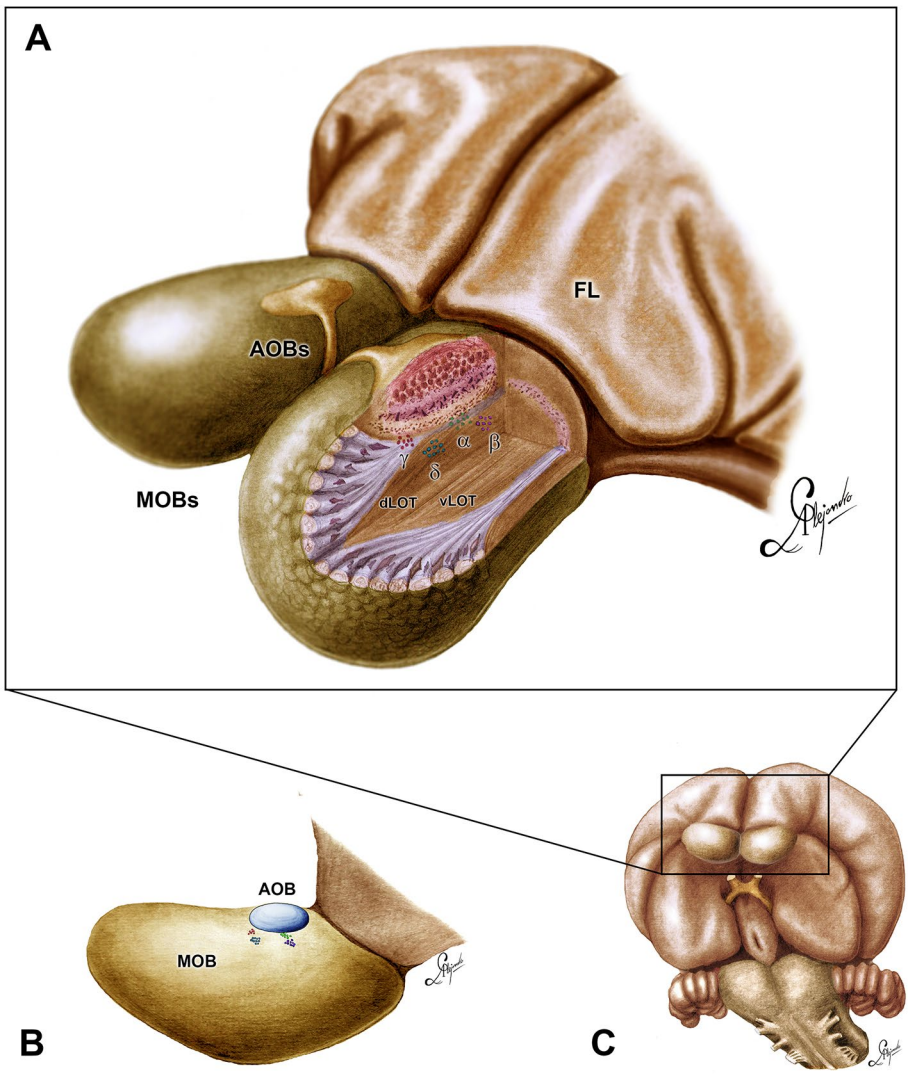

Fig. 10 Drawings of the olfactory bulbs, showing the topographical organisation of the four neuronal clusters identified in the accessory bulbar core white matter. **a** The α and β groups are located parallel to the caudal half of the bulb, whereas the γ and δ groups are beneath the rostral third of the bulb. **b** Schematic drawing of the topographic relationships between the nuclei and the AOB: α (green), β (dark blue), γ (red), and δ (light blue). **c** Rostro-ventral view of the rabbit brain, showing the area depicted in (**a**). *AOB* accessory olfactory bulb, *MOB* main olfactory bulb, *FL* frontal lob, *dLOT* dorsal lateral olfactory tract, *vLOT* ventral lateral olfactory tract

Morphometric and stereological study

There were no sex differences in the volume of the nervous, glomerular, external cellular, and internal cellular of the AOB (see Table 2 and Fig. 14). Additionally, in order to compare the relative volumes of the glomerular layer in both bulbs, a similar morphometric study was done in the MOB. There were again no sex differences in the layer volumes of the MOB except in the deep granule cell layer (Suppl. Material. Table 1 Figure…[EI3]).

The density study (number of neurons per volume unit) of the ECL found significant differences by sex in the neuronal density in the ECL of the AOB. Females showed a greater number of neurons per volume than male rabbits ($t = 2.72$, $P < 0.01$) (Fig. 15).

Discussion

Several developments during the last decades have greatly contributed towards the improving our understanding of the VNS in mammals. Regrettably, these contributions have not been based on the precise knowledge of the neuroanatomical basis of this system, except in laboratory rodents (Takami & Graziadei 1991; Keverne 2002; Larriva-Sahd 2008; Barrios et al. 2014) and opossums (Halpern & Martínez-Marcos 2003) and, beyond mammals, the singular case of the garter snakes (Martínez-Marcos et al. 2002).

There are significant structural, phylogenetic, and species-specific variations among AOB locations, shapes, sizes and morphologic differentiation and development patterns. The AOB can either be perfectly developed (Rodriguez

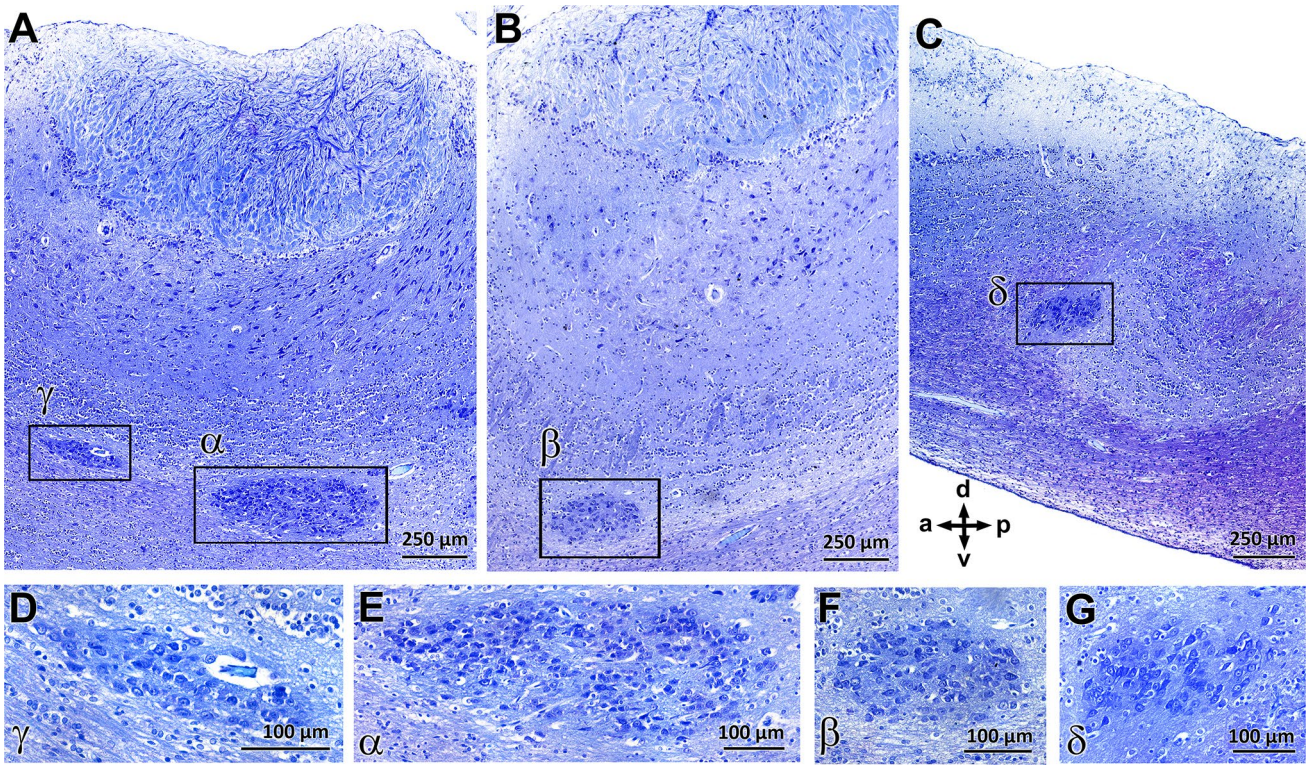

Fig. 11 Three selected photomicrographs of the Nissl-stained sagittal serial sections of the AOB, showing the four neuronal clusters present in the accessory bulbar core white matter. The sections are ordered from medial (**a**) to lateral (**c**). **d–g** Higher magnifications of the four nuclei shown in a–c: γ (**d**), α (**e**), β (**f**), and δ (**g**). *a* anterior, *p* posterior, *d* dorsal, *v* ventral

et al. 1999), poorly differentiated (Nakajima et al. 1998), or entirely absent (Ngwenya et al. 2011) depending on the species.

Although rabbits have become a model for the study of chemocommunication in mammals (Schaal et al. 2003; Schneider et al. 2018), there remains a lack of morphological and immunohistochemical information regarding the structural features of their AOBs. Amusingly, the term "accessory olfactory bulb" was coined by Gudden (1870) after his macroscopic observations of the rabbit olfactory bulb. However, apart from the early microscopic observations reported by Ramón y Cajal (1904), only a few studies feature the AOB more than incidentally (Segovia et al. 2006; Meisami & Bhatnagar 1998; Mori et al. 1987; Schneider et al. 2018).

We have found that the adult rabbit has a fully developed AOB, in terms of size, topography, cell density, as well as the sharpness of the boundaries between AOB layers and its definite antero-posterior zonal organisation. In addition, the shape, size, distribution and arrangement of neurons are all well developed in the rabbit AOB. These features in rabbits can be compared to those found in marsupials, such as opossums (Jia & Halpern 2004), prosimians, such as *Tupaia* (Skeen & Hall 1977), and rodents, such as mouse, rat, and capybara (Salazar et al. 2006; Larriva-Sahd 2008; Suarez et al. 2011b).

To discuss the primary morphological features of the AOB, we have organised the discussion into three sections, moving from superficial to deep: the VNL and GlL; the ECL; and the ICL. We have followed the nomenclature proposed by Larriva-Sahd (2008) whose more significant changes are the introduction of two new layers, an ECL joining the former external granular layer (EGL), mitral-tufted layer (MTL) and EPL, and an ICL replacing the internal granule layer (IGL).

Superficial layers: vomeronasal nerve and glomerular layers

The most superficially located layer (the vomeronasal nerve layer) consists of thick bundles of unmyelinated vomeronasal nerve fibres that open into the deeper GlL. AOB glomeruli consist of an acellular neuropil. When comparing MOB and AOB glomeruli, the appearance of AOB glomeruli is very loose because of their smaller sizes and densely packed arrangement. Additionally, in the MOB, the whole perimeter of the glomeruli is delimited by PG cells, whereas in the AOB these cells are concentrated along the border between the GlL and plexiform layers, forming a very narrow band. This organisation is quite similar to that found in the mouse AOB (Salazar et al. 2006; Yokosuka 2012).

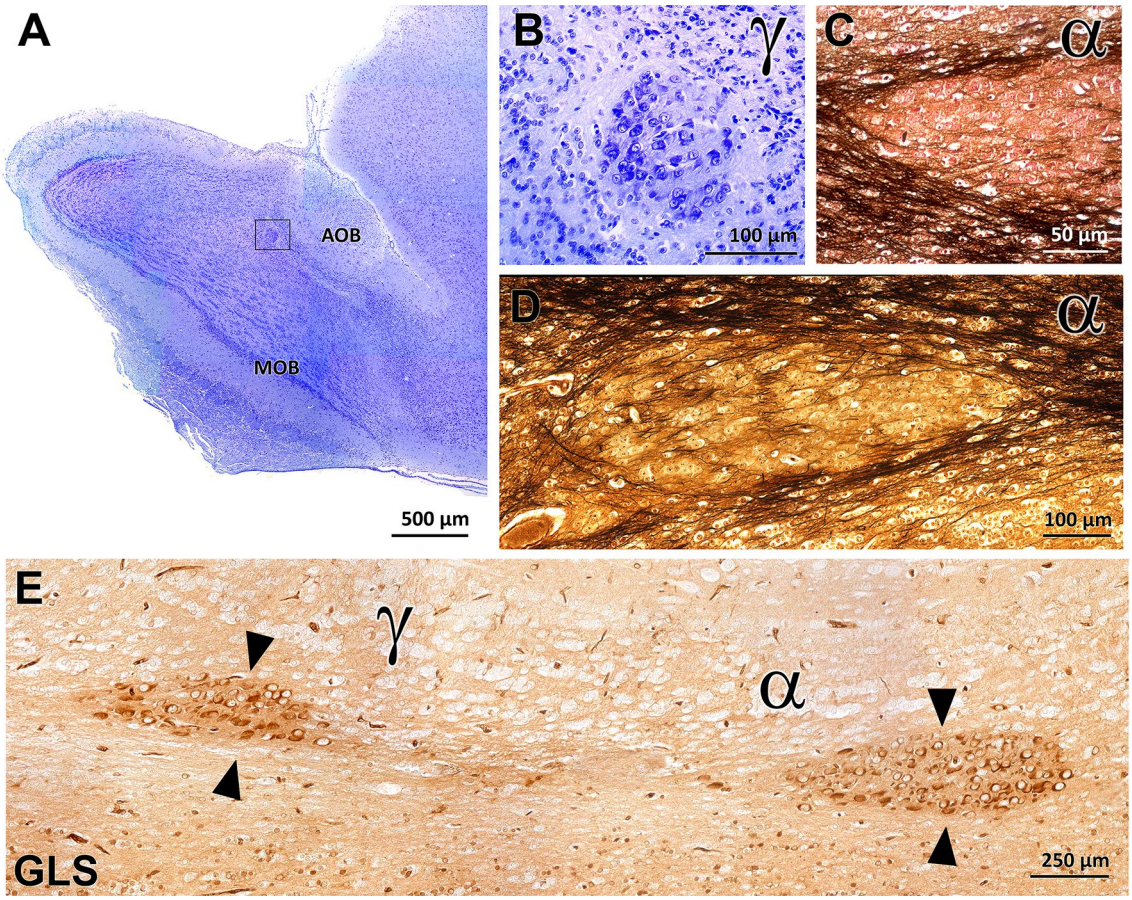

Fig. 12 Histological and immunohistochemical study of the intrabulbar neuronal clusters. **a** Low-power photomicrograph of the Nissl-stained γ group. **b** Higher magnification of the inset from (**a**), showing the cellular organisation of the nucleus. **c** Bielschowsky-stained, pyronin-counterstained, sagittal section of the α group. **d** Bielschowsky-stained section of the α group. **e** Anti-GLS immunohistochemical labelling of the α and γ groups. *a* anterior, *p* posterior, *d* dorsal, *v* ventral, *GLS* glutaminase

The glomerular map in the AOB appears to be more complex than that in the MOB. Wagner et al. (2006) found in mice that inputs from neurons expressing closely related V1Rs intermingle within shared domains of the AOB. At the same time, individual principal cells extend dendrites to glomeruli associated with different, but likely closely related, V1Rs. These features of the glomerular organisation were shown in the rabbit AOB by Mori (1983) who reconstructed a whole dendritic tree of single mitral/tufted cells and verified that it emits two to four stem dendrites that make terminal arborization from three to seven glomeruli.

The nervous fibres in the VNL are enclosed by numerous ensheathing cells, which promote the regenerative abilities of VNL receptor neurons (Chehrehasa et al. 2014). GFAP is a commonly used marker for these cells in mammals and other vertebrates (Lazzari et al. 2016; Smithson & Kawaja 2009). Anti-GFAP immunostaining allowed us to identify the nuclei and the profuse arborization of these cells in the rabbit AOB.

Both superficial layers (VNL and GlL) showed different labelling patterns for immunostaining against Gαi2, Gαo, GAP-43, OMP, CB and CR and for histochemical staining with two of the three lectins, BSI-B_4 and LEA.

The vomeronasal and olfactory receptors are linked to receptor-activated heterotrimeric G proteins (composed of Gα and Gβ/Gγ subunits), which represent important components of the cell signalling cascade in VNO neurons (Dulac & Torello 2003). Thus far, the Gαi2 and Gαo subunits have been associated with the two primary vomeronasal receptor families: V1R and V2R, respectively (Shinohara et al. 1992; Jia & Halpern 1996).

Analyses of G protein distribution, using immunolabelling in the AOBs of several mammals, have shown that V1R-Gαi2 neurons project their axons towards the glomeruli located in the AOB rostral region, whereas the V2R-Gαo neurons project towards glomeruli in the caudal region. This segregated projection within the AOB has been observed in Rodentia (Mouse: Jia & Halpern 1996; rat: Shinohara

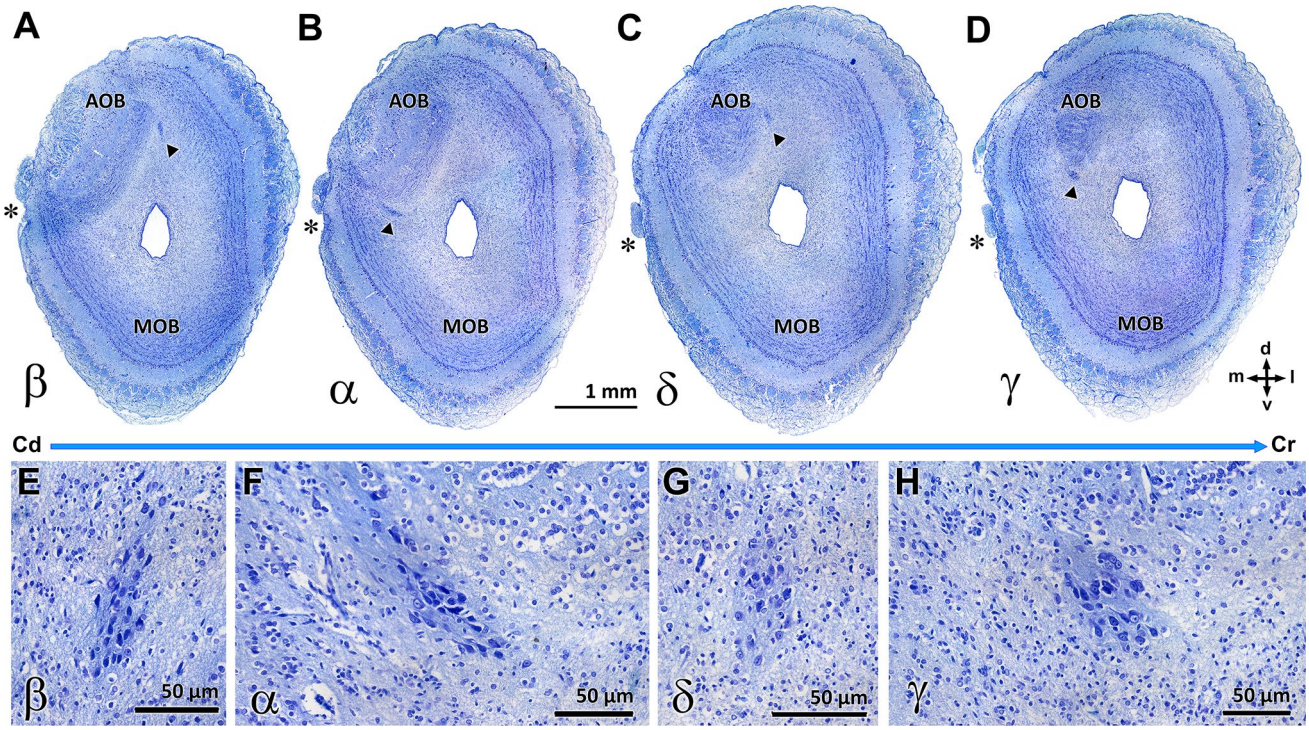

Fig. 13 Four selected photomicrographs of Nissl-stained transverse serial sections of the AOB, containing the four neuronal clusters of the accessory bulbar core white matter. The sections are ordered from caudal (**a**) to rostral (**d**). **e–h** Higher magnifications of the four nuclei shown in a–d: β (**e**), α (**f**), δ (**g**), and γ (**h**). *m* medial *l* lateral, *d* dorsal, *v* ventral, *vomeronasal nerve

Table 2 Sex differences in the volume of the rabbit AOB main layers (in μm^3). Data are expressed as mean ± SEM

	Males	Females
VNL	728,449,498 ± 71,943,802	761,912,023 ± 124,587,198
GlL	859,116,242 ± 129,693,385	786,005,578 ± 107,145,412
ECL	1,602,796,215 ± 124,092,624	1,677,138,884 ± 246,963,840
ICL	1,430,140,439 ± 111,006,803	1,503,304,648 ± 213,078,758

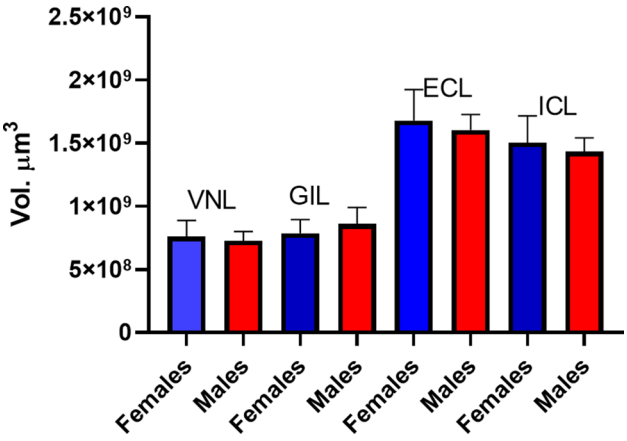

Fig. 14 Morphometric study of the AOB layers volume sexual dimorphism. There were no statistically significant sexual differences. Unpaired Student's *t* test. Data are mean ± SEM; $n = 6$ rabbits per sex. *VNL* vomeronasal nerve layer, *GlL* glomerular layer, *ECL* external cellular layer, *ICL* internal cellular layer

et al. 1992; degu: Suarez & Mpodozis 2009; and capibara: Suarez et al. 2011b), Marsupialia (Opossum: Halpern et al. 1995) and Afrosoricida (Lesser hedgehog tenrec: Suarez et al. 2009). However, it is not a common feature among mammals, and the Gαo pathway is absent in several orders, including Artyodactila (Goat: Takigami et al. 2000), Perysodactila (Horse: Takigami et al. 2004), Carnivora (Dog: Salazar et al. 2013; cat: Salazar & Sanchez-Quinteiro 2011), Insectivora (Musk shrew: Takigami et al. 2004), Primates (Marmoset: Takigami et al. 2004), Hyracoidea (African cape hyrax: Suarez et al. 2011a) and some Rodentia (Squirrels: Suarez et al. 2011a).

Here, we provide the first report of both Gαi2 and Gαo proteins being expressed in the AOB of Lagomorpha. Our previous immunohistochemical contributions to the VNO (Villamayor et al. 2018) showed that in the rabbit vomeronasal sensory epithelium, both Gαi2 and Gαo expressing neurons coexist. However, they do not organise following a zonal pattern of distribution: Gαi2 labels a subpopulation of apical cells, whereas Gαo labels a broader pattern over the whole neuroepithelium. These results contrasted with the well-defined apical Gαi2 and basal Gαo

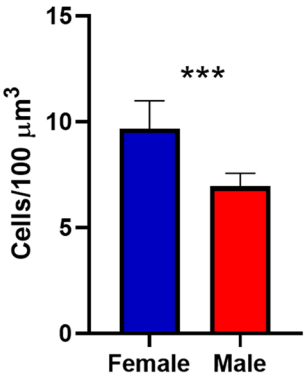

Fig. 15 Stereological study of the sexual dimorphism in the numeric cell density of the principal cells of the ECL of the AOB. There were statistically significant sexual differences. Data are mean ± SEM. Unpaired Student's *t* test. $n = 6$ rabbits per sex. ***$p < 0.01$

pattern found in species such as opossum (Halpern et al. 1995), mouse (Barrios et al. 2014), and rat (Jia & Halpern 1996). Therefore, we addressed the following questions: does the AOB contain both typical Gαo and Gαi2 subclasses of vomeronasal neurons, are these subclasses of neurons segregated in the AOB, and do they follow the same ill-defined pattern observed in the VNO?

Our single- and double-immunohistochemical labelling of G proteins in the AOB has shed light on the distribution of the vomeronasal receptor subclasses in the rabbit AOB. Both antibodies not only discriminate two zones of the AOB but they also follow an anterior–posterior zonation pattern. These immunohistochemical results likely extrapolate to the effective expression patterns of the two families of receptors, V1R and V2R, as occurs in rodents. Thus, Lagomorpha align with the small group of mammalian orders that have two pathways of functional vomeronasal receptors. This molecular finding likely reflects the importance of vomeronasal chemocommunication in rabbits.

Our observations of the G protein expression patterns in the rabbit AOB agree with those obtained by Mori et al. (1987) in the same species using monoclonal antibodies against lactoseries carbohydrates. They found that the R4B12 antibody labelled a subgroup of fibres that ended in the AOB rostrolateral glomeruli, whereas the R5A10 antibody recognised a complementary subgroup of VNNs that is terminated in the AOB caudomedial portion. Although they were unable to determine the functional significance of this heterogeneity at the time, this heterogeneity is now recognised to represent the zonation established by Gαo and Gαi2 proteins and the patterns determined by some glycoconjugates, which have been observed either through the histochemical labelling of lactoseries carbohydrates (Jessell et al. 1990) or through the lectin-histochemical identification of carbohydrate moieties (Shapiro et al. 1995).

Therefore, we also studied the carbohydrates moieties in the rabbit AOB by employing the three lectins most commonly used in both the MOS and the VNS. The functional significance of the sugar residues detected by lectin histochemistry has been suggested to include neurite outgrowth, synaptic plasticity, signal transduction and/or cell–cell interactions (Kinzinger et al. 2005). The affinities with which different lectins bind to the AOB vary among taxa and even among closely related species.

For instance, UEA has been considered to be a specific marker of the vomeronasal pathway (VNO, VNN and AOB) in adult mice (Kondoh et al. 2017; Salazar et al. 2001), whereas the lectin BSI-B_4 has been recognised as an excellent specific marker of the VNS in both rats (Salazar & Sanchez-Quinteiro 1998) and opossums (Shapiro et al. 1995). However, we found that UEA failed to produce labelling in the rabbit AOB and VNNs. This negative pattern has also been found in sheep (Salazar et al. 2000) and Korean roe deer (Park et al. 2014), whereas in other species, such as rats (Salazar & Sanchez-Quinteiro 1998) and pigs (Salazar et al. 2000), UEA labels both the MOS and the AOS.

In rabbits, BSI-B_4 labels both the AOB and the MOB and, therefore, cannot be considered to be a VNS-specific marker. Furthermore, we also studied the LEA labelling pattern in rabbits, and we found that this lectin stains the GlL and nervous layer of both the AOB and the MOB, with a highly conserved pattern, as has been described in a wide range of species, including mouse, sheep, pig, and deer (Salazar et al. 2000, 2001; Park et al. 2014).

Together, these results suggest that glycoconjugates play an important role in primary olfactory and vomeronasal organisation; however, the bases of their detailed expression patterns in every species remain still poorly understood, demonstrating that the diversity among mammalian VNS structures is not only morphological but also neurochemical, physiological, and behavioural.

The antibody against GAP-43 unexpectedly revealed the zonal organisation of the rabbit AOB. Although the anti-GAP43 antibody immunolabelled the entire AOB, we observed that the immunostaining was much stronger within the anterior zone, whereas the posterior zone showed weaker labelling. Thus, both areas were neatly defined. This observation has not been described in any other species for this marker. Additionally, anti-GAP-43 staining established a distinction between the EPL and IPL of the MOB and between the superficial and deep ECL of the AOB.

GAP-43 is a useful probe for discriminating between mature axons and regenerating nerve fibres because its levels in newly formed fibres rapidly decline after the fibres reach their targets (Verhaagen et al. 1989; Ramakers et al. 1992). The olfactory system is an area of the adult nervous system that exhibits extensive synaptic plasticity; therefore, it is not surprising to find a high level of expression for this marker

in the AOB. The zonation observed in rabbits suggests that plasticity is more intense in the anterior AOB than in the posterior AOB.

OMP is another specific marker of the superficial layers of the whole bulb. OMP staining in rabbits was restricted to the nervous strata and the GlLs and was weaker in the AOB than in the MOB. This pattern of labelling is similar to that identified by our group in the neuroepithelium of the rabbit VNO (Villamayor et al. 2018), which was very profuse in both the apical dendrites and axons of the vomeronasal sensory neurons.

Specific immunohistochemical staining for OMP was detected in mature vomeronasal and olfactory receptor-expressing neurons (Farbman & Margolis 1980; Rodewald et al. 2016). Although OMP expression has been studied in a vast range of mammalian VNOs (Dennis et al. 2004, 2019), the study of its immunoreactivity in the AOB has been restricted to rodents, such as mice, rats, and hamsters (Barrios et al. 2014; Jia & Halpern 1996, Kream et al. 1984), marsupials, such as opossums (Shnayder et al. 1993), and sheep (Salazar et al. 2007). Although the function of OMP remains unknown, it is thought to be involved in the maturation of olfactory and vomeronasal neurons (Bock et al. 2006). Accordingly, OMP labelling increases with age in both the VNO and the AOB (Verhaagen et al. 1989; Ramakers et al. 1992).

Calcium-binding proteins are proteins in large quantities in the olfactory bulb. They have been detected in segregated neuronal populations, allowing the distinction among several neurochemical groups within morphologically homogeneous neuronal types. For the first time, we studied the distribution of CB and CR immunoreactivity in the rabbit AOB. In the superficial layer, entire vomeronasal fibres were immunopositive for both markers, producing positive neuropil staining in all glomeruli. In addition, the whole structure displayed a densely stained neuropil, especially for the CR-immunostained samples. However, the PG cells were not immunopositive for either CR or CB, for paraffin-embedded sections and cryostat free-floating sections.

The CR staining pattern observed in rabbits was identical to those observed in rat (Jacobowitz & Winsky 1991) and opossum (Jia & Halpern 2004) and very similar to that found in hedgehog (Briñón et al. 2001), identifying in the latter species a small population of immunopositive cell bodies surrounding the glomeruli without identifying cell processes.

CB labelling in the superficial layers of the AOB showed more significant interspecies differences than CR labelling. For instance, in rats (Porteros et al. 1995) and opossums (Jia & Halpern 2003, 2004) the neuropil was much less stained than in rabbits; however, in both cases, rats and opossums, some individual glomeruli are immunostained and accompanied by isolated positively stained PG cells.

External cellular layer (ECL)

The Nissl histological staining of the rabbit AOB showed a broad and diffuse arrangement of the principal cells. This arrangement does not allow the distinction of the three layers typically found in the MOB: MCL, EPL, and IPL. Therefore, it is more realistic to consider the MCL and the plexiform layers as a single structure, the ECL, similar to that described in the rat and mouse AOB (Larriva-Sahd 2008; Martín-López et al. 2012).

Interestingly, we have observed that the immunohistochemical labelling of GAP-43 in the rabbit could be a useful probe for discriminating both plexiform layers. Principal cells do not express this antibody, either in the soma or in the dendrites, whereas anti-GAP-43 immunostains the plexiform neuropil, following a zonal profile. This profile can easily be observed in the rabbit MOB, where the IPL is strongly marked by the GAP-43-antibody, whereas the EPL is more lightly stained. This pattern makes sense because most of the axons are concentrated in the IPL. This pattern is conserved in the AOB, although the border between the layers is not as neat as in the MOB; however, we can conclude that the existence of two plexiform layers in the AOB is far from a theoretical concept.

Although projecting cells in the AOB share similarities with mitral cells in the MOB, their somata are rarely mitral shaped, and their connectivity is different (Mori, 1983). Thus, the term mitral should be avoided. Accordingly, we adopt the nomenclature proposed by Larriva-Sahd (2008) who described in rat three types of principal cells: large principal cells, round projecting cells and tufted cells. The first of these is by far the most numerous in the rat's olfactory bulb. The rabbit AOB presents a similar cellular diversity in its principal cells, with three cell types morphologically comparable to those present in rats. However, large principal cells do not predominate as much as it happens in rodents (Takami & Graziadei 1991; Larriva-Sahd 2008). The positive immunohistochemical labelling observed for the GLS antibody demonstrates the glutamatergic nature of the rabbit AOB principal cells, similar to the pattern observed for rodents (Quaglino et al. 1999).

Anti-MAP-2 is a useful marker for mitral cell dendritic trees (Dehmelt & Halpain 2005) and it is absent from axons (Bernhardt & Matus 1984). Anti-MAP-2 staining revealed a very dense immunolabelling in the ECL of the rabbit AOB, corresponding to the profuse dendritic trees of principal cells. The MAP-2 immunolabelling also revealed the global contribution of these cells to glomeruli, similar to what has been observed in the mouse AOB (Salazar et al. 2006).

However, in the rabbit AOB the soma of the principal cells was not labelled by anti-MAP-2, whereas in the mouse AOB, principal cell somas were stained by this antibody. This contradictory finding could be explained due to the

slightly different molecular structure of the protein that binds differently to IgG, but more likely reflects specific variations in the distributions of the protein within the soma. AOB principal cells were also negative for calcium-binding protein immunostaining in the rabbit, similar to what has been observed for opossum, rat and mouse (Jacobowitz & Winsky 1991; Jia & Halpern 2004).

Internal cellular layer: Granule cells–White matter α-group of the anterior olfactory nucleus

The granule cells of the rabbit AOB have the same general morphology as those found in the MOB. They are not compactly amassed together, as usually occurs in the AOB of most species (Meisami and Bhatnagar 1998). Instead, the granule cells are grouped into islets, which are very neatly defined by the myelinic fibres of the LOT when visualised using the Bielschowsky method. Both the granule cells and the neuropil are labelled by antibodies against MAP-2, CR, and CB antibodies. The immunolabelling results demonstrate spherical cell bodies and processes that arise and extend toward the superficial regions of the AOB. This pattern is similar to that described in rats, mice, hedgehogs and opossums (Porteros et al. 1995; Jia & Halpern 2004; Briñón et al. 2001).

The axonal fibres projecting from the ECL constitute the contribution of the AOB to the dorsal LOT. In rabbits, these fibres pass through the AOB towards the dorsal LOT which courses under the ICL. This trait has been used as a phylogenetic indicator of common ancestry in mammals (Switzer et al. 1980). This trait is present in most of the Euarchontoglires, a clade of mammals recently defined based on DNA sequence analyses (Murphy et al. 2001) and composed of five groups (Rodentia, Lagomorpha, Dermoptera, Scandentia, and Primatea). In contrast, marsupials, carnivores and ungulates, these fibres pass under the AOB, as observed for the tammar wallaby (Schneider et al. 2012), cat (Salazar & Sanchez-Quinteiro 2011) and roe deer (Park et al. 2014). Our finding confirms the hypothesis established by Schwitzer et al. that, whereas Rodentia has the trait of dorsal LOT fibres passing through the accessory olfactory formation, Lagomorpha represents an intermediate stage in the evolution of this trait.

The deepest layer of the rabbit AOB has an additional striking feature that has received very little attention: the presence, parallel to its ventral segment, of a series of pyramidal-like neuronal clusters that are neatly delimited by the myelinic fibres of the dorsal LOT. One such cluster was first described by Ramón y Cajal in the guinea pig (1904), although he was not able to assign it any function. Lohman (1963) studied these clusters in the guinea pig using Nissl staining, assuming that they belonged to the pars rostralis of the AON. Valverde et al. (1989), in their study on the hedgehog AON, described the presence two similar small cell populations in the bulbar portion of the AON. These populations were, respectively, located in the medial and lateral sections of the dorsal extension of the pars externa of the AON and they were referred to as the α and β groups of the AON. Larriva-Sahd (2012) studied the α-group in rats, mice, and guinea pigs, and reported that the dendrites of these pyramidal-like cells organise into a bundle that ascends to the trigone bounded by the edges of the olfactory limb, the AOB and the dorsal section of the AON. Accordingly, these islands are likely to be functionally related to the sensory qualities detected by both the MOB and AOB.

The only description of this type of cluster in rabbits was reported by Moses Wharton Young (1936), who in his study of the non-cortical centres of the telencephalon of the rabbit included both groups in a schematic transverse drawing of the caudal part of the olfactory bulb. They were described in the text as circular patches of cells in the medial and lateral extremes of the pars dorsalis of the AON. Undoubtedly, these patches are the rabbit equivalents of the α and β groups of the AON that were described by Valverde et al. (1989).

Our sagittal and transverse serial sections of several specimens of the rabbit AOB demonstrate that, in addition to the α and β clusters, the rabbit possesses two clusters topographically related to the anterior AOB, one of which is located medially, whereas the other is found laterally. Following the Valverde criteria, we have named them the γ and δ groups. The anterior positioning of these additional groups makes it very unlikely that they are associated with the AON, supporting the observations of Larriva-Sahd (2012), who associated the α group with the second-order processing of olfactory and vomeronasal information. Future studies should address the roles played by these unique neuronal formations.

Morphometrical study

Although we did not find qualitative histological and immunohistochemical differences between sexes in the rabbit AOB, the morphometric study pointed to the existence of sexual differences. We found that the volume of the female AOB layers was slightly larger than that found in males, apart from the case of the glomerular layer. But, in each case the differences were not statistically significant. Comparing this result with that obtained by Segovia et al. (2006) in their morphometric study of the vomeronasal system of the rabbit, both studies found a similar non-significant tendency.

However, our stereologic study has determined a statistically significant difference between sexes regarding the numerical density of the principal cells within the ECL. The females have greater numerical density values than the males. In this case, although Segovia et al. observed significant sexual differences in the total number of cells

in the mitral cellular layer, the sexual difference values become statistically non-significant when these values were adjusted according to the volume of each layer. Our study, carried out with the same number of animals from both sexes but with a greater number of sections and dissectors, has allowed us not only to confirm the trends found by Segovia et al. (2006) but also to conclude that a statistically significant sexual dimorphism exists in the numerical density of the principal cells of the external cell layer.

Our contribution and the study by Segovia et al. (2006), taken together, make a strong case for the conclusion that the female rabbit AOB presents higher morphometric values than the male. However, in a previous research on the AOB of the rat (Guillamón & Segovia 1997), they found a significant sexual dimorphism, but in this case with greater morphological values in males. There is no explanation for these species differences in the expression of sexual dimorphism, although we agree with Guillamón and Segovia that they are probably a consequence of the reproductive, behavioural, and physiological traits of each species. In that regard, it should be borne in mind that female rabbits are reflex ovulators, while female rats are spontaneous ovulators, and that the sexual and maternal behaviours also differ between the species.

The existence of two divergent patterns in species as close as the rat and the rabbit raises a warning about the risk of extrapolating to other species the findings obtained in rodents on the sexual dimorphism of the brain.

After this exhaustive characterisation of the rabbit AOB, we conclude that the adult rabbit possesses a differentiated and sexually dimorphic AOB, featuring many specific particularities at both the structural and functional levels. These results highlight the significance of chemocommunication in this species, and further anatomical studies that include the connectivity and functional properties of the principal cells of the AOB, as well other parts of the VNS, namely, the vomeronasal amygdala, should be performed. Moreover, given that chemocommunication is especially important during the early stages of life (Schaal et al. 2003), developmental anatomical studies examining the maturity of the rabbit VNS during prenatal and early postnatal stages are also necessary.

Acknowledgements The authors thank COGAL SL (Pontevedra, Spain) for providing most of the animals employed in this study. Special thanks are due to Alejandro García MD, DVM for his artistic drawing of the AOB topography. We also thank Professor Ignacio Salazar, for his support and constant encouragement during his fruitful period as Head of the Department of Anatomy.

Funding This work was supported by a University of Santiago de Compostela grant [1551-8179] to PSQ.

Compliance of ethical standards

Conflict of interest The authors declare that the research was conducted in the absence of any commercial or financial relationships that could be construed as a potential conflict of interest.

Ethical approval All procedures performed in this study involving living animals were in accordance with the ethical standards of the Institutional Animal Care Committee of the Universidad de Santiago de Compostela under procedure number MR110250.

Informed consent No human subject was used in this study.

References

Apfelbach R, Blanchard CD, Blanchard RJ et al (2005) The effects of predator odors in mammalian prey species: a review of field and laboratory studies. Neurosci Biobehav Rev 29:1123–1144

Barrios AW, Nuñez G, Sanchez-Quinteiro P et al (2014) Anatomy, histochemistry, and immunohistochemistry of the olfactory subsystems in mice. Front Neuroanat 8:63

Ben-Shaul Y, Katz LC, Mooney R et al (2010) In vivo vomeronasal stimulation reveals sensory encoding of conspecific and allospecific cues by the mouse accessory olfactory bulb. PNAS 107:5172–5177

Bernhardt R, Matus A (1984) Light and electron microscopic studies of the distribution of microtubule-associated protein 2 in rat brain: a difference between dendritic and axonal cytoskeletons. J Comp Neurol 226:203–221

Bock P, Rohn K, Beineke A et al (2006) Site-specific population dynamics and variable olfactory marker protein expression in the postnatal canine olfactory epithelium. J Anat 215:522–535

Boehm U (2006) The vomeronasal system in mice: from the nose to the hypothalamus- and back! Semin Cell Dev Biol 17:471–479

Bouvier AC, Jacquinet C (2008) Pheromone in rabbits. Preliminary technical results on farm use in France. In: Xiccato G, Trocino A, Lukefahr SD (eds) 9th World rabbit congress. Verona, 2008. Proceedings, pp 303–308

Brennan PA, Zufall F (2006) Pheromonal communication in vertebrates. Nature 444:308–315

Briñón JG, Weruaga E, Crespo C et al (2001) Calretinin-, neurocalcin-, and parvalbumin-immunoreactive elements in the olfactory bulb of the hedgehog (Erinaceus europaeus). J Comp Neurol 429:554–570

Brown RE (1985) Effects of social isolation in adulthood on odor preferences and urine-marking in male rats. Behav Neural Biol 44:139–143

Charra R, Datiche F, Casthano A et al (2012) Brain processing of the mammary pheromone in newborn rabbits. Behav Brain Res 226:179–188

Chehrehasa F, Ekberg JA, St John JA (2014) A novel method using intranasal delivery of EdU demonstrates that accessory olfactory ensheathing cells respond to injury by proliferation. Neurosci Lett 563:90–95

Dehmelt L, Halpain S (2005) The MAP2/Tau family of microtubule-associated proteins. Genome Biol 6:204

Dennis JC, Smith TD, Bhatnagar KP et al (2004) Expression of neuron-specific markers by the vomeronasal neuroepithelium in six species of primates. Anat Rec 281:1190–1200

Dennis JC, Stilwell NK, Smith TD et al (2019) Is the mole rat vomeronasal organ functional? Anat Rec. https://doi.org/10.1002/ar.24060

Dulac C, Torello AT (2003) Molecular detection of pheromone signals in mammals: from genes to behaviour. Nat Rev Neurosci 4:551–562

Farbman AI, Margolis FL (1980) Olfactory marker protein during ontogeny: immunohistochemical localization. Dev Biol 74:205–215

Frahm HD, Bhatnagar KP (1980) Comparative morphology of the accessory olfactory bulb in bats. J Anat 130:349–365

González-Mariscal G, Caba M, Martínez-Gómez M et al (2016) Mothers and offspring: the rabbit as a model system in the study of mammalian maternal behavior and sibling interactions. Horm Behav 77:30–41

Grus WE, Shi P, Zhang Y et al (2005) Dramatic variation of the vomeronasal pheromone receptor gene repertoire among five orders of placental and marsupial mammals. PNAS 102:5767–5772

Gudden B (1870) Experimental untersuchungen über das peripherische und centrale nervensystem. Arch Psychiatr Nervenkr 11:693–723

Guillamón A, Segovia S (1997) Sex differences in the vomeronasal system. Brain Res Bull 44:377–382

Halpern M (1987) The organization and function of the vomeronasal system. Annu Rev Neurosci 10:325–362

Halpern M, Martínez-Marcos A (2003) Structure and function of the vomeronasal system: an update. Prog Neurobiol 70:245–318

Halpern M, Shapiro LS, Jia C (1995) Differential localization of G proteins in the opossum vomeronasal system. Brain Res 677:157–161

Hasui K, Takatsuka T, Sakamoto R et al (2003) Double autoimmunostaining with glycine treatment. J Histochem Cytochem 51:1169–1176

Holy TE (2018) The accessory olfactory system: innately specialized or microcosm of mammalian circuitry? Annu Rev Neurosci 41:501–525

Ihara S, Yoshikawa K, Touhara K (2013) Chemosensory signals and their receptors in the olfactory neural system. Neuroscience 254:45–60

Isogai S, Si S, Pont-Lezica L et al (2011) Molecular organization of vomeronasal chemoreception. Nature 478:241–245

Jacobowitz DM, Winsky L (1991) Immunocytochemical localization of calretinin in the forebrain of the rat. J Comp Neurol 304:198–218

Jessell TM, Hynes MA, Dodd J (1990) Carbohydrates and carbohydrate-binding proteins in the nervous system. Annu Rev Neurosci 13:227–255

Jia C, Halpern M (1996) Subclasses of vomeronasal receptor neurons: differential expression of G proteins (Gi alpha 2 and G (o alpha)) and segregated projections to the accessory olfactory bulb. Brain Res 719:117–128

Jia C, Halpern M (2003) Calbindin D28 k immunoreactive neurons in vomeronasal organ and their projections to the accessory olfactory bulb in the rat. Brain Res 977:261–269

Jia C, Halpern M (2004) Calbindin D28k, parvalbumin, and calretinin immunoreactivity in the main and accessory olfactory bulbs of the gray short-tailed opossum, *Monodelphis domestica*. J Morphol 259:271–280

Keverne EB (2002) Pheromones, vomeronasal function, and gender-specific behavior. Cell 108:735–738

Kinzinger JH, Johnson EW, Bhatnagar KP et al (2005) Comparative study of lectin reactivity in the vomeronasal organ of human and nonhuman primates. Anat Rec 284:550–560

Kondoh D, Kamikawa A, Sasaki M et al (2017) Localization of α1-2 fucose glycan in the mouse olfactory pathway. Cells Tissues Organs 203:20–28

Kream RM, Davis BJ, Kawano T et al (1984) Substance P and catecholaminergic expression in neurons of the hamster main olfactory bulb. J Comp Neurol 222:140–154

Larriva-Sahd J (2008) The accessory olfactory bulb in the adult rat: a cytological study of its cell types, neuropil, neuronal modules, and interactions with the main olfactory system. J Comp Neurol 510:309–350

Larriva-Sahd J (2012) Cytological organization of the alpha component of the anterior olfactory nucleus and olfactory limbus. Front Neuroanat 6:23

Lazzari M, Bettini S, Franceschini V (2016) Immunocytochemical characterisation of ensheathing glia in the olfactory and vomeronasal systems of Ambystoma mexicanum (Caudata: Ambystomatidae). Brain Struct Funct 221:955–967

Lohman AHM (1963) The anterior olfactory lobe of the guinea pig. Acta Anat 45:9–109

Mackay-Sim A, Duvall D, Graves BM (1985) The West Indian manatee (Trichechus manatus) lacks a vomeronasal organ. Brain Behav Evol 27:186–194

Mandiyan VS, Coats JK, Shah NM (2005) Deficits in sexual and aggressive behaviors in Cnga2 mutant mice. Nat Neurosci 8:1660–1662

Martínez-Marcos A, Lanuza E, Halpern M (2002) Neural substrates for processing chemosensory information in snakes. Brain Res Bull 57:543–546

Martín-López E, Corona R, López-Mascaraque L (2012) Postnatal characterization of cells in the accessory olfactory bulb of wild type and reeler mice. Front Neuroanat 6:15

Meisami E, Bhatnagar KP (1998) Structure and diversity in mammalian accessory olfactory bulb. Microsc Res Tech 43:476–499

Melo AI, González-Mariscal G (2010) Communication by olfactory signals in rabbits: its role in reproduction. Vitam Horm 83:351–371

Mohrhardt J, Nagel M, Fleck D et al (2018) Signal detection and coding in the accessory olfactory system. Chem Senses 43:667–695

Mombaerts P (2004) Genes and ligands for odorant, vomeronasal and taste receptors. Nat Rev Neurosci 5:263–278

Mori K (1983) Mitral cells in the rabbit accessory olfactory bulb: their morphology and response to LOT stimulation. Soc Neurosci Abst 9:1020

Mori K (1987) Monoclonal antibodies (2C5 and 4C9) against lactoseries carbohydrates identify subsets of olfactory and vomeronasal receptor cells and their axons in the rabbit. Brain Res 408:215–221

Mori K, Imamura K, Fujita SC et al (1987) Projections of two subclasses of vomeronasal nerve fibers to the accessory olfactory bulb in the rabbit. Neuroscience 20:259–278

Mouton PR (2002) Principles and practices of unbiased stereology. An introduction for bioscientists. John Hopkins University Press, Baltimore

Murphy WJ, Eizirik E, O'Brien SJ et al (2001) Resolution of the early placental mammal radiation using Bayesian phylogenetics. Science 294:2348–2351

Nakajima T, Sakaue M, Kato M et al (1998) Immunohistochemical and enzyme-histochemical study on the accessory olfactory bulb of the dog. Anat Rec 252:393–402

Ngwenya A, Patzke N, Ihunwo AO et al (2011) Organisation and chemical neuroanatomy of the African elephant (*Loxodonta africana*) olfactory bulb. Brain Struct Funct 216:403–416

Pardo-Bellver C, Martínez-Bellver S, Martínez-García F et al (2017) Synchronized activity in the main and accessory olfactory bulbs and vomeronasal amygdala elicited by chemical signals in freely behaving mice. Sci Rep 7:9924

Park C, Ahn M, Lee JY et al (2014) A morphological study of the vomeronasal organ and the accessory olfactory bulb in the Korean roe deer, *Capreolus pygargus*. Acta Histochem 116:258–264

Porteros A, Arévalo R, Crespo C et al (1995) Calbindin D-28k immunoreactivity in the rat accessory olfactory bulb. Brain Res 689:93–100

Pro-Sistiaga P, Mohedano-Moriano A, Ubeda-Bañon I et al (2007) Convergence of olfactory and vomeronasal projections in the rat basal telencephalon. J Comp Neurol 504:346–362

Quaglino E, Giustetto M, Panzanelli P et al (1999) Immunocytochemical localization of glutamate and gamma-aminobutyric acid in the accessory olfactory bulb of the rat. J Comp Neurol 408:61–72

Ramakers GJ, Verhaagen J, Oestreicher AB et al (1992) Immunolocalization of B-50 (GAP-43) in the mouse olfactory bulb: predominant presence in preterminal axons. J Neurocytol 21:853–869

Ramón y Cajal S (1904) Corteza Olfativa. In: Textura del Sistema Nervioso Central del Hombre y los Vertebrados, vol 2. Imprenta y Librería Nicolas Moya, Spain, pp 913–941

Ramos-Vara JA, Miller MA (2006) Comparison of two polymers based immunohistochemical detection systems: ENVISION + and ImmPRESS. J Microsc 224:135–139

Rodewald A, Gisder D, Gebhart VM et al (2016) Distribution of olfactory marker protein in the rat vomeronasal organ. J Chem Neuroanat 77:19–23

Rodriguez I, Feinstein P, Mombaerts P (1999) Variable patterns of axonal projections of sensory neurons in the mouse vomeronasal system. Cell 97:199–208

Rodriguez I, Greer CA, Mok MY et al (2000) A putative pheromone receptor gene expressed in human olfactory mucosa. Nat Genet 26:18–19

Salazar I, Sanchez-Quinteiro P (1998) Lectin binding patterns in the vomeronasal organ and accessory olfactory bulb of the rat. Anat Embryol 198:331–339

Salazar I, Sanchez-Quinteiro P (2011) A detailed morphological study of the vomeronasal organ and the accessory olfactory bulb of cats. Microsc Res Tech 74:1109–1120

Salazar I, Sanchez-Quinteiro P, Cifuentes JM et al (1998) The accessory olfactory bulb of the mink, *Mustela vison*: a morphological and lectin histochemical study. Anat Histol Embryol 27:297–300

Salazar I, Sanchez-Quinteiro P, Lombardero M et al (2000) A descriptive and comparative lectin histochemical study of the vomeronasal system in pigs and sheep. J Anat 196:15–22

Salazar I, Sanchez-Quinteiro P, Lombardero M et al (2001) Histochemical identification of carbohydrate moieties in the accessory olfactory bulb of the mouse using a panel of lectins. Chem Senses 26:645–652

Salazar I, Sanchez-Quinteiro P, Cifuentes JM et al (2006) General organization of the perinatal and adult accessory olfactory bulb in mice. Anat Rec 288:1009–1025

Salazar I, Sanchez-Quinteiro P, Alemañ N et al (2007) Diversity of the vomeronasal system in mammals: the singularities of the sheep model. Microsc Res Tec 70:752–762

Salazar I, Cifuentes JM, Sanchez-Quinteiro P (2013) Morphological and immunohistochemical features of the vomeronasal system in dogs. Anat Rec 296:146–155

Sam M, Vora S, Malnic B et al (2001) Odorants may arouse instinctive behaviours. Nature 412:142

Schaal B, Coureaud G, Langlois D et al (2003) Chemical and behavioural characterization of the rabbit mammary pheromone. Nature 424:68–72

Schneider NY, Fletcher TP, Shaw G et al (2012) Goα expression in the vomeronasal organ and olfactory bulb of the tammar wallaby. Chem Senses 37:567–577

Schneider NY, Piccin C, Datiche F et al (2016) Spontaneous brain processing of the mammary pheromone in rabbit neonates prior to milk intake. Behav Brain Res 313:191–200

Schneider NY, Datiche F, Coureaud G (2018) Brain anatomy of the 4-day-old European Rabbit. J Anat 232:747–767

Segovia S, Garcia-Falgueras A, Carrillo B et al (2006) Sexual dimorphism in the vomeronasal system of the rabbit. Brain Res 1102:52–62

Shapiro LS, Ee PL, Halpern M (1995) Lectin histochemical identification of carbohydrate moieties in opossum chemosensory systems during development, with special emphasis on VVA-identified subdivisions in the accessory olfactory bulb. J Morphol 224:331–349

Shinohara H, Asano T, Kato K (1992) Differential localization of G-proteins Gi and Go in the accessory olfactory bulb of the rat. J Neurosci 12:1275–1279

Shnayder L, Schwanzel-Fukuda M, Halpern M (1993) Differential OMP expression in opossum accessory olfactory bulb. NeuroReport 5:193–196

Skeen LC, Hall WC (1977) Efferent projections of the main and the accessory olfactory bulb in the tree shrew (Tupaia glis). J Comp Neurol 172:1–35

Slotnick B (2001) Animal cognition and the rat olfactory system. Trends Cogn Sci 5:216–222

Smithson LJ, Kawaja MD (2009) A comparative examination of biomarkers for olfactory ensheathing cells in cats and guinea pigs. Brain Res 1284:41–53

Sterio DC (1984) The unbiased estimation of number and sizes of arbitrary particles using the disector. J Microsc 134:127–136

Suarez R, Mpodozis J (2009) Heterogeneities of size and sexual dimorphism between the subdomains of the lateral-innervated accessory olfactory bulb (AOB) of Octodon degus (Rodentia: Hystricognathi). Behav Brain Res 198:306–312

Suarez R, Villalón A, Künzle H et al (2009) Transposition and Intermingling of Galphai2 and Galphao afferences into single vomeronasal glomeruli in the Madagascan lesser Tenrec *Echinops telfairi*. PLoS ONE 4:e8005

Suarez R, Fernández-Aburto P, Manger RR et al (2011a) Deterioration of the Gαo vomeronasal pathway in sexually dimorphic mammals. PLoS One 6:e2643

Suarez R, Santibáñez R, Parra D et al (2011b) Share and differential traits in the accessory olfactory bulb of caviomorph rodents with particular reference to the semiaquatic capybara. J Anat 218:558–565

Swaney WT, Keverne EB (2009) The evolution of pheromonal communication. Behav Brain Res 200:239–247

Switzer RC 3rd, Johnson JI, Kirsch JA (1980) Phylogeny through brain traits. Relation of lateral olfactory tract fibers to the accessory olfactory formation as a palimpsest of mammalian descent. Brain Behav Evol 17:339–363

Szendrő Z, Szendrő K, Zotte AD (2012) Management of reproduction on small, medium and large rabbit farms: a review. Asian-Australas J Anim Sci 25:738–748

Szendrő Z, Mikó A, Odermatt M et al (2013) Comparison of performance and welfare of single-caged and group-housed rabbit does. Animal 7:463–468

Takami S, Graziadei PP (1991) Light microscopic Golgi study of mitral/tufted cells in the accessory olfactory bulb of the adult rat. J Comp Neurol 311:65–83

Takigami S, Mori Y, Ichikawa M (2000) Projection pattern of vomeronasal neurons to the accessory olfactory bulb in goats. Chem Senses 25:387–393

Takigami S, Mori Y, Tanioka Y et al (2004) Morphological evidence for two types of Mammalian vomeronasal system. Chem Senses 29:301–310

Tolivia J, Tolivia D, Navarro A (1998) New technique for differential staining of myelinated fibers and nerve cells on paraffin sections. Anat Rec 222:437–440

Trinh K, Storm DR (2003) Vomeronasal organ detects odorants in absence of signaling through main olfactory epithelium. Nat Neurosci 6:519–525

Trotier D, Eloit C, Wassef M et al (2000) The vomeronasal cavity in adult humans. Chem Senses 25:369–380

Trouillet AC, Keller M, Weiss J et al (2019) Central role of G protein Gαi2 and Gαi2 + vomeronasal neurons in balancing territorial and infant-directed aggression of male mice. PNAS 116:5135–5143

Valverde F, López-Mascaraque L, De Carlos JA (1989) Structure of the nucleus olfactorius anterior of the hedgehog (Erinaceus europaeus). J Comp Neurol 279:581–600

Vega MD, Barrio M, Quintela LA et al (2012) Evolución del manejo reproductivo en cunicultura. ITEA 108:172–190

Verga M, Luzi F, Carenzi C (2007) Effects of husbandry and management systems on physiology and behavior of farmed and laboratory rabbits. Horm Behav 52:122–129

Verhaagen J, Oestreicher AB, Gispen WH et al (1989) The expression of the growth associated protein B50/GAP43 in the olfactory system of neonatal and adult rats. J Neurosci 9:683–691

Villamayor PR, Cifuentes JM, Fdz-de-Troconiz P et al (2018) Morphological and immunohistochemical study of the rabbit vomeronasal organ. J Anat 233:814–827

Wagner S, Gresser AL, Torello AT et al (2006) A multireceptor genetic approach uncovers an ordered integration of VNO sensory inputs in the accessory olfactory bulb. Neuron 50:697–709

Wharton Young M (1936) The nuclear pattern and fiber connections of the non-cortical centers of the telencephalon of the rabbit (*Lepus cuniculus*). J Comp Neurol 65:295–401

Wyatt TD (2003) Pheromones and animal behaviour: communication by smell and taste. Cambridge University Press, Cambridge

Wysocki CJ (1979) Neurobehavioral evidence for the involvement of the vomeronasal system in mammalian reproduction. Neurosci Biobehav Rev 3:301–341

Yokosuka M (2012) Histological properties of the glomerular layer in the mouse accessory olfactory bulb. Exp Anim 61:13–24

Yoon H, Enquist LW, Dulac C (2005) Olfactory inputs to hypothalamic neurons controlling reproduction and fertility. Cell 123:669–682

Zufall F, Leinders-Zufall T (2007) Mammalian pheromone sensing. Curr Opin Neurobiol 17:483–489